HHS Public Access

Author manuscript

Neuroimage. Author manuscript; available in PMC 2019 September 01.

Published in final edited form as:

Neuroimage. 2018 September ; 178: 210–223. doi:10.1016/j.neuroimage.2018.05.038.

Mutual Connectivity Analysis of Resting-State Functional MRI Data with Local Models

Adora M. DSouza[a,1,*], **Anas Z. Abidin**[b], **Udaysankar Chockanathan**[c], **Giovanni Schifitto**[d,e], and **Axel Wismüller**[a,b,e,f,1]

[a]Department of Electrical Engineering, University of Rochester, Rochester, New York, USA

[b]Department of Biomedical Engineering, University of Rochester, Rochester, New York, USA

[c]Department of Biochemistry and Biophysics, University of Rochester Medical Center, Rochester, New York, USA

[d]Department of Neurology, University of Rochester Medical Center, Rochester, New York, USA

[e]Department of Imaging Sciences, University of Rochester, NY, USA

[f]Faculty of Medicine and Institute of Clinical Radiology, Ludwig Maximilians University, Munich Germany

Abstract

Functional connectivity analysis of functional MRI (fMRI) can represent brain networks and reveal insights into interactions amongst different brain regions. However, most connectivity analysis approaches adopted in practice are linear and non-directional. In this paper, we demonstrate the advantage of a data-driven, directed connectivity analysis approach called Mutual Connectivity Analysis using Local Models (MCA-LM) that approximates connectivity by modeling nonlinear dependencies of signal interaction, over more conventionally used approaches, such as Pearson's and partial correlation, Patel's conditional dependence measures, etcetera. We demonstrate on realistic simulations of fMRI data that, at long sampling intervals, i.e. high repetition time (TR) of fMRI signals, MCA-LM performs better than or comparable to correlation-based methods and Patel's measures. However, at fast image acquisition rates corresponding to low TR, MCA-LM significantly outperforms these methods. This insight is particularly useful in the light of recent advances in fast fMRI acquisition techniques. Methods that can capture the complex dynamics of brain activity, such as MCA-LM, should be adopted to extract as much information as possible from the improved representation. Furthermore, MCA-LM works very

[*]Corresponding author. adora.dsouza@rochester.edu (Adora M. DSouza).

[1]Both authors contributed equally

Author contributions

A. M. DSouza conceptualized and designed the work, collected, analyzed and interpreted the data, and wrote the paper. A. Abidin contributed to the data collection, software and analysis support, and contributed to reviewing the paper. U. Chockanathan contributed to reviewing the paper. G. Schiffito provided expert knowledge and contributed to the collection of the data. A. Wismüller invented the MCA-LM method and contributed to reviewing the paper.

well for simulations generated at weak neuronal interaction strengths, and simulations modeling inhibitory and excitatory connections as it disentangles the two opposing effects between pairs of regions/voxels. Additionally, we demonstrate that MCA-LM is capable of capturing meaningful directed connectivity on experimental fMRI data. Such results suggest that it introduces sufficient complexity into modeling fMRI time-series interactions that simple, linear approaches cannot, while being data-driven, computationally practical and easy to use. In conclusion, MCA-LM can provide valuable insights towards better understanding brain activity.

Keywords

Resting-state fMRI; functional connectivity; BOLD fMRI; hemodynamic response; repetition time

1. Introduction

The investigation of intrinsic, spontaneous fluctuations observed in a resting human brain from functional connectivity analysis of fMRI scans has demonstrated that the brain inherently organizes itself into functional networks even at rest [1]. This seminal work was a strong impetus to the growth of resting-state functional connectivity analysis [2, 3, 4, 5, 6, 7] by providing a gateway to revealing information about underlying brain functioning. Since then, the dynamics of the brain, at both rest and under the influence of an activation paradigm, has been a widely-studied topic [8, 9, 10, 11]. The estimation of connectivity first requires defining a set of nodes in the brain which have an associated fMRI time-series such as the activity of regions of interests (ROIs) or single voxels. Subsequently, connections between these nodes (known as edges) are established based on directed or undirected (e.g. correlation) connectivity. Analyzing this data can reveal valuable information about the underlying dynamics of the brain. To this end, studies on functional integration, i.e. understanding interaction between different regions in the brain have been carried out [12, 13]. Functional integration can be obtained using functional and/or effective connectivity analysis [14, 15]. Succinctly, functional connectivity analysis captures the statistical association between neurophysiological time-series, whereas effective connectivity analysis captures coupling or directed information flow between regions [14], most commonly using a priori models of interactions. Here, we use mutual connectivity analysis (MCA) [16] which estimates a form of directed functional connectivity by estimating mutual cross-prediction between time series through state space reconstruction.

Functional MRI (fMRI) non-invasively captures brain activity by measuring the blood oxygen level dependent (BOLD) response to neural activity, which is a complex function of the metabolic rate of oxygenation, cerebral blood volume and cerebral blood flow [17]. Furthermore, fMRI time-series have been shown to exhibit dynamic non-linear behavior both in the presence of activation paradigms [18, 19] and at rest [20, 21]. However, a majority of functional connectivity literature has focused on linear techniques, such as correlation and partial correlation. One of the first few approaches that modelled the nonlinear brain dynamics was Dynamic Causal Modeling (DCM) [9]. DCM, which is an effective connectivity analysis approach, estimates neuronal interactions using a priori information about the intrinsic physiology to model neuronal activity from the recorded

fMRI time-series. Such an approach can model causal interactions between neurons. However, this is achieved at the cost of having to estimate a large number of parameters [7]. It is inherently a hypothesis-driven data modeling approach that uses the data to validate a prior hypothesis. In contrast, data-driven, model-free approaches discover patterns from the data itself and are more flexible than model-based methods.

Nonlinear data-driven approaches applied on fMRI data do not assume prior knowledge about the model driving a system and capture the signal dynamics without explicitly modeling the hidden neuronal state. A few such nonlinear data-driven methods for fMRI functional connectivity analysis have been proposed [22, 23]. We have recently introduced an approach called Mutual Connectivity Analysis (MCA) to quantify the nonlinear association between fMRI time-series in brain [16]. MCA constructs non-linear function approximators between every pair of time-series and tries to learn a mapping from one time-series to another. The more accurate the cross-prediction from a given function approximator is, the more closely the time-series interact. We have previously demonstrated the applicability of MCA with generalized radial basis function neural networks and Local Models (LM) [16, 24]. In this paper, in contrast to previous publications, we perform a systematic evaluation of MCA-LM by testing it against realistic simulated fMRI [25] and compare it with more conventionally used approaches, such as Pearson's and partial correlation, mutual information, Granger causality, coherence measures and Patel's conditional dependence measures.

The use of nonlinear dynamic models to establish a measure of directed interaction between time-series has recently been applied in various domains, such as complex ecological systems [26], gene regulatory networks [27] and electroencephalography (EEG) [28]. Also, it has been discussed in [10, 21] that the brain dynamics may not be very different from other complex, nonlinear, dynamical systems such as those encountered in nature. As such, we have adopted this knowledge to model the brain dynamics using concepts from complex system theory to study connectivity in the brain with MCA-LM. Predictive modeling based on MCA-LM does not require sophisticated assumptions on the intrinsic mechanism of the signal being studied. It can hence provide a non-linear, data-driven approach to estimate connectivity from the BOLD fMRI signals. Each fMRI time-series can be represented by a state space, which is reconstructed from time delayed versions of itself and embedded into a state-space reconstruction (SSR) without any prior information of an exact model of its dynamics. Such a space of embedded points transforms the observed time-series into a manifold [29, 30, 31, 32] representing the evolution of states, i.e. its dynamics. The basic idea of such a non-linear time-series analysis scheme is to build local models of the state space dynamics for every fMRI time-series, which cross-predicts the trajectory of an influencing time-series. Although a wide range of local models have been described in time-series literature [33], we focus on establishing connectivity as a measure of influence quantified by the cross-prediction between every pair of time-series using nonlinear weighted local average models [34, 26]. Such a weighting has been demonstrated to work well for ecological data [26] as well as electrocorticography ECoG data from monkeys [35].

In this work, we investigate the applicability of MCA-LM in fMRI analysis, i.e. MCA-LM, to detect interactions on realistic fMRI simulations as proposed by [25]. Their study

evaluated a wide range of network modeling methods with realistic fMRI simulations and has shown that, in general, correlation-based approaches and Bayes nets are quite effective in detecting presence of network connections regardless of direction. However, the estimation of directionality appears as a more challenging task, where most of the studied methods performed poorly, with Patel's conditional independence performing the best amongst the tested methods. In [36], the authors showed that by performing group-level analysis, many of the Bayesian approaches performed well at estimating causal interactions. However, analysis at single subject level using these approaches did not perform as well [37]. In this paper, we investigate the use of MCA-LM to capture the presence of directed connections in simulated fMRI data as proposed in [25]. Furthermore, we study the effect that different sampling rates (repetition times) have on MCA-LM and various correlation-based approaches.

We test MCA-LM under different conditions of simulated time-series generation which include 1) varying TR, 2) varying connection strength of neural interactions, 3) varying noise, 4) varying number of nodes, and 5) various network graph structures. In the following sections, we: 1) discuss the data used, both simulated and real resting-state fMRI, 2) give a brief overview of MCA-LM and the other approaches evaluated, 3) apply these methods on the realistic fMRI simulated data and study MCA-LM performance under various simulation settings, 4) investigate the applicability of MCA-LM to extract relevant connections from empirical resting-state fMRI data performing connectivity analysis of subnetworks within the Default Mode Network (DMN).

2. Materials

2.1. Simulated fMRI time-series

The simulation of fMRI data requires mathematical formulations about physiological and environmental influences affecting neuronal activity and the observed BOLD fMRI signals. To accomplish this task, we adopted the network structure designed by [25], where the resting-state fMRI time-series were modelled by simulating neuronal activity based on dynamic causal modeling [9] which was then passed through a non-linear balloon model [8] to estimate its vascular dynamics. The neural signal interaction was defined by the network connections in A. The neural network model was defined as:

$$\dot{z} = \sigma A z + C u \quad (1)$$

where z is the neural time-series and $\dot{z}$ is the rate of change of the neural time-series z, A is the network matrix, which is the ground truth of neural connections in this model, C is the matrix defining external connections, u are external connections, and σ controls the temporal smoothing and neural lag within-node and between nodes. Further details on the simulation can be found in [25]. All parameters apart from the TR and connection strength were adopted from [25]. Table 1 describes the various network structures and simulation parameters used. Figure 1 is an example of a ground truth network A (networks #4 and #12 from Table 1). Network topologies for all other simulations can be found in Figure 2.

We generated a number of simulations at different parameter settings, because we were interested in studying, how the performance of the methods were affected by such changes. A summary for all the simulations is provided in Table 1. For all simulations, i.e. sim#1 to sim#13 we investigated the effect of scan TR. We evaluated the methods on simulations obtained at TR = {0.5 s, 1 s, 1.5 s, 2 s, 3 s}. Ideally, a connectivity analysis approach should be scalable and work for large networks having many nodes as well as small networks. Sim#1 has 5 nodes, sim#4 has 50 nodes, while sim#2 and sim#3 have a number of nodes in between 5 and 50, Table 1. Sim#5 models bidirectional, inhibitory as well as excitatory connections (conn.) between nodes. Accounting for such connections is important, since in the brain it is rare that two regions are only influenced by undirected, excitatory connections. Sim#6 reflects inaccurate regions of interest (ROI) characterization. One of the most common pre-processing steps in the fMRI literature is to divide the brain into a number of ROIs. Inaccurate ROI representation presents a unique challenge, since this would result in mixing of the BOLD signal across regions. We were also interested in investigating, if MCA-LM could characterize cyclic connections as such networks theoretically cannot be recovered using Bayes net methods. Sim#7 models such cyclic connections. The network structure of sim#8 is very dense, which simulates a small network that is highly connected. More details about these simulations can be found in [25]. Furthermore, simulations sim#9 through sim#13 were obtained using the same network structure as sim#1 to sim#5, with the only difference being that they were generated at moderate connection strength of neuronal interaction while the others were generated at weak neuronal connection strength. Both types of strengths were sampled from a Gaussian distribution, to model neuronal interactions, with standard deviation of 0.1; mean = 0.4 (with range limited between 0.2–0.6) for moderate, and mean = 0.2 (with range limited between 0.15–0.25) for weak, connection strength. The distribution of moderate interaction strengths was adopted from [25] and used in [36, 38]. This was extended to model weak interactions. For all edges, this introduced small perturbation of edge strengths, which can be thought of as representing noise in the neuronal connection strength across trials.

With these simulations, we varied the number of nodes, similar to studies by [38, 36, 25], scan TR [39] and added thermal noise with standard deviation between (0.1% – 1%) of the signal [25], these factors and network structure are summarized in Table 1. In addition to these parameters, we also varied the strength of neuronal connection, examined networks with cyclic connections, dense networks and networks with bi-directional, forward and backward connections [25]. We studied the effect of weak and moderate connection strength of neuronal interaction. Fifty different trials for every network structure were generated. Each trial for a given model had the same network structure and parameters (number of nodes, TR, noise, etc.) as shown in Table 1, but had different neural time-series, HRF parameters (standard deviation of 0.5 s), and connection strengths. The connection strengths were varied between trials, within the limits described previously, to account for noise and possible difference between multiple fMRI recordings. However, the network structure was the same between trials. In total we tested 90 different simulation models, each with 50 trials, obtained from combinations of parameters as described in Table 1. It should also be mentioned here that we do not perform high-pass filtering as was done in [25]. It was shown

in [40] that this step eliminates non-Gaussian information in the signal which can be useful in estimating direction.

2.2. Empirical resting-state fMRI data

Functional MRI (fMRI) data from 14 healthy subjects, was acquired using a 3.0 Tesla Siemens Magnetom TrioTim scanner at the Rochester Center for Brain Imaging (Rochester, NY, US). Two scans were acquired from the subjects within the span of an hour. The study protocol included: (i) High-resolution structural imaging using T1-weighted magnetization-prepared rapid gradient echo sequence (MPRAGE, TE = 3.44 ms, TR= 2530 ms, isotropic voxel size 1mm,ip angle = 7).(ii) Resting-state fMRI scans using a gradient spin echo sequence (TE = 23 milliseconds, TR = 1650 milliseconds, 96 × 96 acquisition matrix, ip angle of 84). The acquisition lasted 6 minutes and 54 seconds, and 250 temporal scan volumes were obtained. A total of 25 slices, each 5 mm thick, were acquired for each volume. During acquisition, the subject was asked to lie down still with eyes closed. The data were acquired as part of a NIH sponsored study (R01-DA-034977). The individual had given written consent as per IRB approved study protocol.

Prior to computation of connectivity, the fMRI data used in this study was preprocessed using standard methodology. For each dataset, the first ten (of 250) volumes of functional magnetic resonance images were removed to analyze only those in which steady-state imaging had been reached. Next, motion correction, brain extraction and correction for slice timing acquisition were performed. Additional nuisance regression, to remove variations due to head motion and physiological processes was carried out. This model included linear and quadratic trends, signals from white matter and cerebrospinal fluid using CompCor [41], and the Friston-24 motion parameters (Friston et al., 1996). Each dataset was finally registered to the 2 mm MNI standard space using a 12-parameter affine transformation. All preprocessing steps were carried out using the C-PAC software [42] and its corresponding dependencies in FMRIB Software Library(FSL) [43]. Finally, the time-series were normalized to zero mean and unit standard deviation to focus on signal dynamics rather than amplitude [44].

3. Methods

3.1. Connectivity measures

Figure 3 illustrates how connectivity analysis summarizes information in the large number fMRI time-series recorded over multiple time points.

3.1.1. Pearson's Correlation—Correlation is a measure of the linear statistical association between two time-series. We use the Pearson correlation coefficient, which is the most widely used correlation approach for fMRI functional connectivity analysis. The Pearson correlation, referred to here as full correlation (FC), normalizes the covariance of the two time-series by the product of their standard deviation.

3.1.2. Partial Correlation—Partial correlation (PC) quantifies a measure of interaction between two time-series controlled for the effects of other series in the system. PC is useful in a multivariate, setting as it is better able to distinguish between direct and indirect

connections unlike full correlation. Say that the PC between two time-series, **x** and **y**, is to be obtained for a system with N time-series. PC achieves this by first regressing out the information of all the other $N-2$ time-series in the system from **x** and **y** followed by correlating these regressed time-series with each other. Since it is a computationally expensive task to solve many multiple regression problems, the covariance matrix inversion approach is used to obtain the full set of partial correlations [45].

3.1.3. Patel's conditional dependence measures—Patel's conditional dependence measures the imbalance between $P(\mathbf{x}|\mathbf{y})$ and $P(\mathbf{y}|\mathbf{x})$ to measure connectivity [46]. We adopt the approach used by [25] where each time-series is mapped to the range 0–1. From the normalized time-series, we extract Patel's κ and Patel's τ measures which quantify connection and directionality respectively. We also binarise the data at thresholds of (0.25, 0.5, 0.75 and 0.9). However, we only report results on the continuous data and data thresholded at 0.25 since other thresholds gave poor results. We use the naming convention: Patel τ and Patel κ for the connectivity matrices calculated on continuous data while Patel25 τ and Patel25 κ is calculated on binarized data. Directed connectivity matrices obtained from κ and τ are called Patel directed and Patel25 directed. Further details are provided in the supplementary material.

Additionally, we investigate multivariate Granger causality [47], mutual information [48] and coherence [49] approaches, details of which are provided in the supplementary material.

3.1.4. Mutual connectivity analysis: Local Model—Nonlinear modeling methods have the ability to characterize complex brain dynamics and reveal useful insights into the underlying functional architecture of the brain. To this end, we adopt a powerful technique from dynamical systems theory to reconstruct the state space and perform predictions using local models. In the following paragraphs, we describe mathematical formulations adopted from [26]. The convention used is: scalars - lowercase italics, vectors - lowercase boldface, matrices - uppercase boldface, matrices of dimension higher than 2 - uppercase boldface italicized. For example, time-point t of time-series **x** is given by the scalar $x(t)$.

Consider a dynamical system with two time-series, **x** and **y**, sharing an attractor manifold [29, 30, 31, 32], representing the state space (phase space) of the system. If **y** influences **x**, estimates of the states of **y** can be obtained from that of **x**, but not vice versa, unless **x** influences **y** [26]. A measure of causation is established with local models, where, the signature of the influencing time-series **y** is looked for in the influenced series **x**. This is done by quantifying the correspondence between the libraries of nearby points in the attractor manifold built from **x** to that built from **y**. Details about the construction of such manifolds are given in the subsequent paragraph. To put this simply, a measure of the estimation quality of **x** cross-predicting **y** is related to the influence **y** has on **x** [26].

Using delay-coordinate embedding, time series **x** is represented as a d-dimensional mapping, i.e. manifold, $\boldsymbol{M}_{\mathbf{x}}$. $\boldsymbol{M}_{\mathbf{x}}$ is constructed using vectors $\mathbf{x}_t = [x(t-(d-1)), \ldots, x(t-1), x(t)]$, and $t \in d, \ldots, T$. To obtain a cross-prediction of **y** denoted as $\hat{\mathbf{y}}|\boldsymbol{M}_{\mathbf{x}}$ (where, $\hat{\mathbf{y}}|\boldsymbol{M}_{\mathbf{x}}$, is the estimate of **y** obtained using $\boldsymbol{M}_{\mathbf{x}}$) at a point t, i.e. $\hat{y}(t)|\boldsymbol{M}_{\mathbf{x}}$, we obtain the $d+1$ nearest neighbors of $\mathbf{x}_t$,

whose time-indices are used to identify nearest neighbors of $y(t)$ and obtain an estimate $\hat{y}(t)|\boldsymbol{M}_{\mathbf{x}}$ as follows:

$$\hat{y}(t)|\boldsymbol{M}_{\mathbf{x}} = \sum_{i=1}^{d+1} w_i y(t_i) \quad (2)$$

The cross-predicted estimate of $\hat{y}(t)|\boldsymbol{M}_{\mathbf{x}}$ is established with weighted average local models to detect non-linear dynamics derived from time delay-coordinate embedding. The weights, w_i ($i \in 1, \ldots, d+1$), are determined by a softmax, function such that the first nearest neighbor $\mathbf{x}_{t_1}$ of $\mathbf{x}_t$ has the highest weight,

$$w_i = \frac{e^{-\|\mathbf{x}_t - \mathbf{x}_{t_i}\|^2 / \|\mathbf{x}_t - \mathbf{x}_{t_1}\|^2}}{\sum_{j=1}^{d+1} e^{-\|\mathbf{x}_t - \mathbf{x}_{t_j}\|^2 / \|\mathbf{x}_t - \mathbf{x}_{t_1}\|^2}} \quad (3)$$

If **y** influences **x**, the nearest neighbors of $\boldsymbol{M}_{\mathbf{y}}$ should correspond to those of $\boldsymbol{M}_{\mathbf{x}}$ (Figure 4), and hence a good estimate of **y** should be obtained. A similarity measure using correlation is calculated between the estimated $\hat{\mathbf{y}}|\boldsymbol{M}_{\mathbf{x}}$ and the original time-series **y**, which quantifies the ability of **x** to cross-predict **y**. The measure of cross-prediction quantifies a directed non-linear measure of interaction, which is stored in an affinity matrix **S**, at matrix element $\mathbf{S}_{(\mathbf{x},\mathbf{y})}$. Similarly, a measure of cross-prediction between each time-series pair is obtained. Further details can be found in [26].

We establish a measure of mutual connectivity, which quantifies the non-linear mutual cross mapping between every pair of time-series on the reconstructed state space with local models (LM). Such cross-maps establish a measure of nonlinear association between every pair of time-series in a dynamic system. These measures, used to construct connectivity profiles for every trial, quantify the underlying dynamics of the simulated resting-state fMRI. The embedding dimension $d = 3$ is chosen using Cao's method [50].

The weighting function adopted here in eq 3 is user-specified. It is the same as that used in [26] that studies dynamical systems in ecology and in [35] that investigates brain activity in monkeys from Electrocorticography (ECoG) data. This approach is termed local models since the model for every state is constructed locally with only neighborhood of points. Local models for every state of the predictor are created by searching for its nearest neighbors in the state space, as such every state has a different set of nearest neighbors and a different weight. The closest neighbor is given the highest weight, while the furthest is assigned the least weight.

3.2. Simulated fMRI data

Connectivity matrices obtained using all the methods are estimated for all the simulations summarized in Table 1.

3.2.1. Evaluation and summary of simulation results—Table 1 summarizes all the simulation models used in this study. Note that for every simulation, the TR and/or noise varies. For example, sim#9 has 10 different sub-models. To simplify the discussion of results, we use the following naming conventions - all simulations of #n, n ∈ {1, 2, …, 13} are sim#n and specific sets of parameters for sim#n are $\text{sim\#n}_{(\text{TR;noise})}$ (all other parameters for sim#n are a constant). Example: $\text{sim\#9}_{(1.5,0.1)}$ refers to simulation #9 at TR = 1.5 s and noise = 0.1%.

In this paper, we study the effectiveness of MCA-LM in estimating interaction scores in a network under different time-series generation schemes and evaluate it against conventionally used approaches. MCA-LM is evaluated in its ability to quantify presence of connection regardless of direction in terms of c-sensitivity [25, 38]. This is done by symmetrizing the directed matrices [25] by considering the maximum of the two directed connections between nodes as the edge strength. C-sensitivity quantifies how well the true positives (TP) are separated from the false positives (FP) by measuring the fraction of TPs that are estimated with a higher connection strength than the 95th percentile of the FP distribution.

For every simulation model, the 50 iterations are summarized as a boxplot (example: Figure 5). The circle with a dot inside the box represents the distribution median. The box spans the first quartile to the third quartile which is interquartile range (IQR). The vertical extensions from the box, whiskers, have a maximum length of 1.5 times the IQR. We test for significant differences between MCA-LM and the other methods with the Wilcoxon signed-rank test. A significant difference ($p < 0.01$) is indicated by a × sign in the plot. Inspection of the plots can reveal whether MCA-LM is significantly better or worse than the other approaches. The median of the c-sensitivity is represented as $\tilde{c}_{method}$, where *method* refers to the analysis method used, eg - MCA-LM, FC, PC, etc.

In addition to testing its ability to estimate a presence of a link, we measure MCA-LM's ability in establishing direction by quantifying both, directional information and presence of a true connection with the Area Under the receiver operating characteristic Curve (AUC) and compare it with Patel's conditional independence measures [46]. The Receiver Operating Characteristic (ROC) is a plot of the true positive rate (TPR) versus the false positive rate (FPR), which shows the tradeoff between these quantities. Ideally, TPR should be 1 and FPR = 0 for any particular threshold applied on the connectivity graphs, i.e. affinity matrix, this corresponds to an AUC = 1. An AUC of 0.5 represents random connections. Since the AUC quantifies both, the strength of connections and the direction of information flow, it is used to evaluate performance in estimating the true network structure.

3.3. Application to empirical fMRI data

3.3.1. Default mode network connectivity—We analyze specific interactions obtained within the default mode network (DMN) and performed test-retest reliability to study the robustness of all the approaches. Recently the role of the DMN in the human brain, especially during rest, has gained significant research attention [51, 52, 53, 54]. Abnormalities in the DMN have been characterized in a wide range of neurological diseases such as Alzheimers disease [55], schizophrenia [56], autism [57] and traumatic brain injury

[58, 59, 60, 61, 62] to name a few. In addition, efforts to study connectivity within the DMN has grown [53, 63].

In this paper, we perform a preliminary analysis on the resting-state fMRI data of 14 subjects as described in section 2.2 to explore directed connectivity within the DMN. We divide the DMN of each subject into eight subnetworks, i.e., the precuneus/posterior cingulate cortex (PC/PCC), medial prefrontal cortex (MPFC), left and right inferior parietal lobe (lIPL, rIPL), left and right temporal cortex (lTC, rTC) and left and right medial temporal lobes (lMTL, rMTL) [53, 63]. Each subnetwork was obtained adopting a methodology similar to [64, 53]. To localize subnetworks in the DMN, first, Independent Component Analysis (ICA) is performed using the GIFT toolbox [65] resulting in 60 components. Subsequently, the best spatially matching component to the subnetworks of the DMN is obtained, where, the subnetworks are defined combining regions from the automatic anatomical labeling (AAL) atlas [66] as described in [53]. A nonlinear template matching procedure [64, 67] was adopted, where the maximum of the difference between the average z-scores within the template (DMN subnetwork defined using the AAL template) and the average z-scores outside the template indicated the best component for the given template. For each subject, estimates of activity from the best fitting DMN subnetworks are identified by voxels exhibiting local maximum z-score of the independent component [53].

Measures of test-retest reliability are obtained by correlating connectivity scores of the two sequences for every subject, thus quantifying a measure of robustness of a connectivity analysis.

4. Results

4.1. Simulated fMRI

In this section, we present results on the simulated fMRI data and empirical data. For the simulations, we begin by presenting results in terms of c-sensitivity, followed by Area under the ROC curve. Subsequently, sensitivity and specificity measures are obtained from recovered graphs. For the empirical data, we quantify measures of robustness for all the approaches investigated.

Figure 5 compares performance of simulations 1 to 4 for different settings of TR. Observe that MCA-LM performs significantly better than either of the correlation based approaches, both Patel's kappa methods, coherence based methods and Granger causality analysis (see supplementary material for GC and Coherence results) for TR ≤ 2 s in most of the results. For the four simulations shown in Figure 5, at TR ≤ 2 s, MCA-LM ($\tilde{c}_{LM} \geq 0.82$ for all the 4 simulations) performs better than or on par with methods compared. At TR = 3 s its performance degrades a bit but is still comparable to the methods tested, with median dropping to 0.70 for the 50 node network.

For the 50-node model (sim#4) at TR = 0.5 s, $\tilde{c}_{LM} = 0.95$, $\tilde{c}_{FC} = 0.77$, $\tilde{c}_{PC} = 0.67$, $\tilde{c}_{Patel\kappa} = 0.75$ and $\tilde{c}_{Patel25\kappa} = 0.79$. Correlation based methods and Patel's coefficients are not affected much by the increase in TR. However, there is a steady drop in performance of MCA-LM with increasing TR. Note that with increasing the number of nodes, performance of MCA-

LM does not reduce much as compared to other approaches Figure 6. This figure captures the effect of network size on estimation of connections. Observe that at low TR (TR < 2 s) the drop in MCA-LMs performance is not as significant as the drop in performance of the other approaches when increasing the network size from 5 to 10. However, at TR = 3 s, network size seems to affect MCA-LMs performance.

MCA-LM performs considerably better than the other approaches for sim#5, which is the simulation with backward connections, as seen in Figure 7. Note from Figure 7, $\tilde{c}_{LM} = 1$ for all TRs. Correlation, PC and Patel's coefficients perform quite poorly with median c-sensitivity ≤ 0.6 while Granger causality, mutual information and coherence methods produce a c-sensitivity ≤ 0.4 for all TR values. This is an important result with potentially significant biomedical implications, because in brain networks it is rare to have two regions having connections in only one direction and hence, a simulation with backward connections is more realistic. Results for simulations 6 to 8 for all approaches are in the supplementary material, Figure S2, S6. The general trend observed across all simulations is that the MCA-LM performs better than the other approaches for all TRs in measuring the presence of connection regardless of direction. Furthermore, if the Regions of Interest (ROIs) are poorly defined, sim#6 all the approaches perform poorly as seen in the supplementary material Figure S2, S6.

Simulations 9–13 were obtained for moderate strength (0.2–0.6) of neuronal interaction. Figure 8 shows the results for sim#9–12, where, these simulations at noise = 0.1% are different from sim#1–4 only in strength of connections, all the other parameters were the same (Tabel 1). Notice that with an increase in connection strength, the performance of FC, PC and Patel's measures (Granger causality, mutual information and coherence, Figure S7) increases as compared to lower connections Figure 5 (Figure S5). However, no such increase is observed for MCA-LM and although some methods, particularly partial correlation, perform significantly better than MCA-LM at moderate connection strengths, MCA-LM still performs well for TR < 2 s. Figure comparing performance for different connection strengths is provided in the supplementary material Figure S4. Sim#9–12 results at noise = 1% follow a very similar trend as simulations with lower noise where c-sensitivity decreases with TR and are shown in Figure S2 and S8 of the supplementary material. However, at higher noise, the drop in performance with increased TR is more than that at lower connection strength.

Sim#13 is obtained for the same network structure as sim#5 but at a higher neural connection strength. MCA-LM performs much better than the other approaches for sim#13, which has both inhibitory and excitatory connections, for all TRs studied. Increasing noise degrades its performance but it is still better than the other approaches. The number of indirect connections increases with backward connections hence, full correlation performs poorly. In addition, PC and Patel's measures perform poorly as well. Note from Figure 9, $\tilde{c}_{LM} = 1$ for noise at 0.1% and TR ≤ 2 s. Also, FC and PC perform quite poorly at median c-sensitivity of 0.6 or just under it for all TR and both noise levels. While Patel's coefficients show the poorest performance at median c-sensitivity between 0.4–0.5 for all TR values.

Figure 10 demonstrates the applicability of MCA-LM to recover presence and direction of connections. It is compared with Patel's measure of conditional dependence. Details of how the directed Patel's measure is calculated is provided in the supplementary material S3. For MCA-LM, the AUC drops with increasing TR. However, it is always better than Patel's measures. At all TRs studied, the AUC > 0.90 in all but one simulation, i.e. sim#6 corresponding to bad ROI definition.

Since the measures in Figure 10 does not provide a visualization of the results, we obtained one from average affinity matrices for simulations 1 through 13. Figure 11 shows the graphs obtained using the thresholded average affinity matrices for the simulations at TR = 2 s, where the threshold was applied at $p < 0.01$ under the null hypothesis. MCA-LM measures between non-interacting pairs of surrogate time-series, generated with the Iterative Amplitude Adjusted Fourier Transform (IAAFT) algorithm [68], gave the null distribution. We use the Chaotic Systems Toolbox [69] to generate the surrogates. The green arrow indicates detection of a right connection, while the red arrow indicates the false detection of non-existent connection. Figure 11 suggests that MCA-LM effectively identifies the presence and absence of connections. Figure 12 is the average specificity and sensitivity measures obtained for all the simulations with MCA-LM and Patel25 directed matrix. Since Patel25 performed better that Patel's directed matrix, we have not included it in the results. Table S1 details the sensitivity and specificity for all the simulations.

4.1.1. Empirical data—To demonstrate the applicability of MCA-LM in quantifying resting-state fMRI connectivity profiles and extracting useful information about interaction patterns from the underlying dynamics of the human brain, we tested its performance on empirical rs-fMRI.

Default Mode Network Connectivity—We evaluated the robustness of all the methods investigated by testing reproduciblity of the DMN connectivity profiles estimated by each of the methods on two fMRI sequences of the 14 subjects. Two connectivity matrices, corresponding to each of the sequences, were obtained for every subject and each connectivity analysis method.

Results as of test-retest reliability are shown in Figure 13, where a measure of robustness for each connectivity analysis approach is obtained by correlating the two vectorized connectivity matrices for every subject. For MCA-LM, we show the results for both, symmetrized and non-symmetrized matrices and for Patel's measure we present results on Patel's κ, which is a symmetric measure, and directed matrices obtained using Patel's κ and τ. We observe that, FC, PC, Patel's κ are quite robust however, none of these approaches are significantly better than symmetrized MCA-LM. Comparing the directed matrices, i.e., MCA-LM with Patel directed and Patel25 directed (Figure 13), we see that on average, MCA-LM does perform better, however, significant differences using Wilcoxon signed rank test were not observed between MCA-LM and Patel's measures.

Figure 14 plots the average amount every node is influence by every other node in the DMN. Where influence or directionality from **x** to **y** was quantified from the connectivity matrix using: $\mathbf{S}_{(x,y)} - \mathbf{S}_{(y,x)}$ [35]. The average amount every region is influenced is given in Figure

14. A negative value indicates that the region is more of an influencer than one that is influenced.

Studies have shown that the PC/PCC is the core hub in the DMN, and that it is a central node in the DMN [53]. MCA-LM indicates that it is a strongly influenced node, while Patel's measure capture contradictory information between its two measures. Additionally, Patel's measure indicate that the rMTL is the most influenced while the lTC is the most influencing node.

5. Discussion

In this study, we investigate the applicability of MCA-LM to analyze realistic simulated and empirical fMRI data. The premise for performing such an analysis was that conventionally used linear methods of modeling functional interactions in the brain, such as correlation-based approaches, fall short in their ability to capture directed, nonlinear dependencies in dynamic systems such as the brain. Moreover, full correlation cannot distinguish between direct and indirect connections. Additionally, connectivity estimates captured by full correlation, partial correlation and Patel's conditional dependence measures do not improve with reduction in TR as our results suggest, indicating the inability of such standard methods to improve with better image acquisition techniques. For correlation based methods, this can be attributed to the simplistic nature of linear approaches, which in general, only provide a gross approximation of nonlinear processes. As discussed in [70], full correlation is quick to estimate and robust mathematically but is simplistic, however more complex methods that model biophysiological processes, such as DCM, [9] falls short when the number of regions/voxels to be studied grows. Furthermore, Patel's measures may be limited by the need to binarize the time-series data. Additionally, good estimation with Patel's measures requires that the non-directed measures be estimated well first, which may not always be the case as seen for networks with both inhibitory and excitatory connections Figure 7 and 9). To bridge this gap, MCA-LM, introduces sufficient complexity in modeling time-series interactions by estimating nonlinear dynamics and providing a measure of causality which can be extended to large-scale brain networks. Additionally, in contrast, to other approaches it can extract useful information with improvement in the data representation. This is particularly important in the light of advancement in fMRI systems, where systems with temporal resolution of 200 ms [71] and more recently, 80 ms [72] have been developed.

MCA-LM, estimates causal interactions by quantifying the one-to-one mapping of predictor series states to states of predicted series. Here, states are reconstructed using lagged coordinates of the time-series. In short, MCA-LM tests if two time series belong to a common dynamical system. Additionally, MCA-LM estimates states of time-series and does not forecast system evolution through time, eliminating information loss in nonlinear systems [26]. The primary difference between MCA-LM and other lag-based approaches, such as Granger causality, is that it estimates states of say time-series **y** from **x** without using the past information of **y** and only instantaneous and lagged versions of **x**. Here, if **x** predicts **y** well, it implies that **y** causes **x** [26] which may seem counterintuitive to Grangers definition of causality but the fundamental difference lies in not using the past of the time-series to be predicted. Additionally, MCA-LM can model nonlinear dynamics in systems

and may have an edge over Granger causality since it also uses instantaneous information of the predictor time-series which can be helpful to model differential systems observed more commonly in nature.

Essentially, analysis of the realistic simulated data in our study suggests that more complex, nonlinear modeling of dynamic systems such as the brain can reveal useful information and improve connectivity estimates as the sampling rate (repetition time, TR) decreases. In addition, we demonstrate its applicability in estimating connectivity from real resting-state functional MRI data.

Effect of TR

The repetition time (TR) is the length of time between two excitation pulses, i.e., it is the time interval between two consecutive scans of a point in the brain. The TR is directly related to the temporal resolution. As such, for a given scan duration, the reconstructed manifold space becomes less dense and less representative of the true manifold with increasing TR. Hence, increasing the TR has deleterious effects on the estimation of connections between time-series using MCA-LM. This decrease in MCA-LM performance with higher TR is a common trend evident from all the results. However, it still outperforms the other approaches even with the performance reduction at higher TR. Additionally, our results suggest that MCA-LM can potentially extract more meaningful information from improved data representation at low TR. There is a strong push to improving TR and shorter TRs are rapidly becoming the standard in resting-state fMRI analysis as is evident by the efforts of various neuroimaging projects (example - WU-Minn Human Connectome Project (HCP)). Hence, with improvements in scanning technology, non-linear approaches to estimating connectivity, such as MCA-LM, in the brain will find greater applications. Approaches such as correlation, partial correlation, coherence, mutual information, Patel's measures do not improve with reduction in TR. However, Granger causality measures do improve with reduction in TR. Hence, they may find potential use for data acquired at low TR.

Effect of strength of connections

Comparing results in Figure 5 and Figure 8 at noise = 0.1 %, sim#1 and sim#9 respectively, which have the same model generation settings apart from the strength of connections, we note that MCA-LM is robust to reduction in the connection strength. However, the performance drops for other approaches with lower strength of neuronal interaction. MCA-LM's ability to capture connections in weakly linked systems could be useful as we do not exactly know the strength at which neurons interact. Even if the strength of influence of one time-series on another is low, the dynamics of the influencing time-series is embedded in the influenced one [26] which is captured by MCA-LM since it models the states of the time-series. However, we observe that with regards to estimating influence at higher connection strength, MCA-LM and Patel's measure have a poor specificity, Figure 12. This indicates that more false positives are detected when connections strength of neuronal interactions are high. Upon further investigation and as evident from Figure 11, at high strengths, bidirectional connections were captured. Analyzing the connectivity matrices estimated by MCA-LM we observed that, for unidirected connections, although the strength of

connections was higher in the direction of influence than in the opposite direction, significance testing detected both connections. MCA-LM was better able to capture direction in weak neuronal interactions, Figure 11.

Estimating backward connections

Simulations 5 and 13 are constructed having bidirectional influences, where influence is excitatory in one direction and inhibitory in the other [25]. This is inline with the current understanding that the connections in the brain constitute of inhibitory and excitory signals. Hence, such a simulation is a more realistic representation of the brain dynamics. A remarkable boost in performance (Figure 7 and Figure 9) with MCA-LM is found over the other approaches. We analyzed the connectivity matrices obtained with all the methods to understand why correlation-based approaches performed so poorly. It appears that using correlation-based methods for a pair of time-series having both inhibitory and excitatory connections, the inhibitory connection (example from time-series **a** to **b**) was acting counter to the excitatory connection (from **b** to **a**). Since, correlation-based approaches and Patel's κ measure cannot disentangle determining a measure of interaction from **a** to **b** and **b** to **a** like MCA-LM, it establishes a low interaction between the two time-series. However, for time-series that only had either excitatory or inhibitory connections between them, these approaches were able to capture a strong connection.

Cyclic connections, dense connections, poor ROI definitions and direction of connection

MCA-LM can capture the presence of connections, as evidenced by the high c-sensitivity in networks with cyclic connections and dense connections, performing similar to the other approaches. Another interesting model studied is the effect poor ROI definitions have on the detection of connections. In many fMRI analysis, spatial ROIs are used to divide the brain into a number of functional regions. However, such spatial ROIs do not necessarily match with the actual functional boundaries. With such an ROI definition, all methods perform very poorly.

With regards to direction of connections, MCA-LM is able to capture the direction of connections well as illustrated in Figures 10 and 11 as shown in Supplementary material Table 1 and 2. The AUC quantifies both, the detection of the presence and the direction of connections as one measure. MCA-LM performs favorably for all TRs. We note that apart from detecting a few wrong connections for the simulation with poor ROI definition and the simulation with dense connections, MCA-LM is able to detect connections well, as shown in Figure 11. In addition, it is able to detect the correct direction of connections for the cyclic graph, which is theoretically not possible using Bayesian approaches. These results underscore the effectiveness of MCA-LM in quantifying connections in a network. Interestingly, the connectivity matrices estimated with Patel's measure perform well only for simulations generated with high strength of connections.

Apart from the methods analyzed in this paper, many approaches to estimate directed connectivity have been proposed literature. Especially in analyzing Electroencephalography (EEG), Magnetoencephalography (MEG) and fMRI data. However, approaches that work well with EEG/MEG data do not necessarily capture directed connectivity well on fMRI

data [73]. This can be attributed to the fact that fMRI is an indirect, smoothened measure of neuronal activity. As such, although there is a vast amount of literature that suggests directed connectivity approaches can quantify causal interactions in EEG/MEG, before applying them to fMRI data, proper validation needs to be carried out with fMRI simulations. In this work, we investigate approaches that are commonly applied to analyze fMRI data. We will also make available the simulations, which can act as a large test bed to validate different connectivity analysis approaches.

Applicability of MCA-LM analyzing empirical fMRI data

All the analyses discussed so far were carried out on simulations of fMRI time-series. However, we also investigated the spontaneous activity at a regional level in the default mode network from empirical resting-state fMRI data in the human brain. Since MCA-LM is a nonlinear data-driven approach, it does not assume prior knowledge about the model driving the dynamics of the system and captures signal dynamics without explicitly modeling the hidden neuronal states.

Previous studies have investigated functional interactions between subnetworks in the DMN [53] using partial correlation. In this study we investigate the robustness of connectivity analysis approaches in estimating connectivity profiles for different fMRI scans of every subject. Higher the similarity of connectivity profiles for the two scans, more robust the connectivity analysis approach. Our results suggest that MCA-LM is quite robust in uncovering the underlying network structure for individuals as evident from the correlation of connectivity profiles between the two runs.

We perform a connectivity analysis on the default mode network (DMN) and compare the resulting interactions with those established in the literature. In recent work [27, 26], it was demonstrated that a good cross-prediction with non-linear predictors was indicative of the presence of a causal influence from the predicted time-series to the predictor series. Using this concept, we provide a means to establish a form of influence to study interactions within the DMN, Figure 14. Our results (Figure 14) are in agreement with studies establishing functional connectivity of the DMN [53], demonstrating the central role of the precuneus/posterior cingulate cortex in the DMN. This is complementary to the fact that PC/PCC has a high metabolic rate [51], is anatomically highly connected [74] and is known to play a central role in the DMN [75]. It is yet to be understood whether the PC/PCC is strongly influenced or a strongly influencing node, and although MCA-LM indicates that the PC/PCC is a highly influenced node, one Patel's measure suggests that it is weakly influenced and the other Patel's measure implies that it is an influencing node. These contradictory results indicate that on real fMRI data, directional analysis should be taken with a grain of salt. A larger cohort of subjects may give more conclusive results.

Limitations and Future work

In this study, we investigate the performance of various connectivity analysis approaches and compare it with a novel technique of using state space reconstruction from time-series to estimate connectivity, i.e. MCA-LM. We see that MCA-LM performs better than the best approaches determined in Smith et al 2011, [25], with the exception of weak performance at

high noise level and high TR. In this study we do not explore Bayesian approaches as proposed in [36], which have shown to work really well on the NetSim data [25], because such are particularly suited to performing group level inference rather than subject level. However the methods we have focused on in this work, do not use prior information from other subjects for inferring connectivity. With this study, we have shown that nonlinear state space modeling performs well on simulations and empirical data. An advantage of subject level connectivity analysis approaches, such as those investigated in this paper is that, these methods can be used when data is limited. In a future study we will compare subject level methods to group level Bayesian approach if data from multiple subjects is available.

One of the shortcomings of MCA-LM is its performance in the presence of noise. It uses local neighborhood information in estimating a time-series. This is sensitive to noise. A more robust model would be one that smoothens the state space thus being less sensitive to noise. Additionally, here, we use equation 3 to as the weighting function, which was also used in [26] and [35]. Another interesting research question would be whether using a different weighting function would produce better results.

Additionally, it has been shown that the brain works at multiple timescales [76, 77, 78], MCA-LM can be modified to account for different timescales by using a different embedding dimension d for the time-series. However, to test the impact of a non-optimal d on performance, we performed a preliminary analysis on the simulated data to test the effect of a higher d ($d = 6$), higher than the optimal we used, on the performance of MCA-LM. We observed that apart for a small drop in performance at higher TR (TR < 2 s) for a few simulations, the performance of MCA-LM was not significantly affected. This is observation is in line to the findings by Huanfei et al., 2014 [27]. Such a result is encouraging, since 1) it demonstrates the robustness of MCA-LM to parameters whose optimum can probably never be really known, additionally, 2) it also shows that even though the brain works at different timescales [76, 77, 78], selecting one d, that is not the optimal, will not deteriorate results significantly.

Analyzing results on simulations helps to understand a method's advantages and disadvantages. However, it is also important to test the approach on empirical data. This is a challenging task since with empirical data we do not have a ground truth of connections. Test-retest reliability gives a measure of robustness of a method, however, it does not help determine if connections estimated are close to the truth. A possible truth can be obtained from fMRI task sequences as a study demonstrates [73]. This can help validate our approach more effectively on empirical data, especially since there would exist known directional relationships.

In summary, MCA-LM is able to estimate a measure of connectivity in different simulation scenarios as well in empirical resting-state fMRI data. It outperforms correlation-based methods, Patel's conditional dependence measure, Granger causality and mutual information for most simulations. We observe that, for a given scan duration, performance of MCA-LM in estimating connections improves with decreasing TR. This is primarily because of two reasons 1) with decreasing TR the number of temporal samples increases and the reconstructed manifold space becomes more dense. 2) At lower TR, the distance between

consecutive time points decreases, resulting in better representation of signal states. Therefore, with improvements in fMRI technology [71, 72], methods that are able to capture the complex dynamics of the brain should be sought after and investigated so as to extract as much information as possible from the improved representation of the brain activity. This study aims to introduce one such approach, i.e. MCA-LM to extract true network connectivity from fMRI data. We have provided the analysis software on our lab website.

6. Conclusion

Mutual connectivity analysis using Local Models (MCA-LM) is a nonlinear modeling approach that extracts meaningful information from fMRI time-series without pre-specification of network parameters. Unlike other non-linear methods of establishing connectivity that start from sophisticated model hypothesis on neural activity, hemodynamic response or cerebral blood flow using different priors, MCA-LM captures and learns useful information from the data itself without requiring potentially inaccurate assumptions about specific network architectures. Such an approach introduces sufficient complexity into modeling fMRI time-series interactions that simple, linear approaches cannot, while not encountering issues concerning increased network models to be pre-specified with more nodes; hence making them computationally practical, easy to use as well as capable of aid in estimating directed connections.

Our results on both the realistic simulated and empirical human resting-state fMRI time-series reveal that MCA-LM can derive useful information from the data. With improvements in image acquisition rates, i.e. reduced TR, its performance improves, whereas other more commonly used approaches cannot exploit the improved time-series representation to derive better connectivity estimates. Our results suggest that such a nonlinear modeling of interactions, based on state space reconstruction, should be applied on data especially for data captured at low TR. In addition, MCA-LM appears robust in physiologically realistic scenarios that affect the captured fMRI data, such as: low connection strength of neuronal interactions, presence of inhibitory connections, dense connection patterns and cyclic connections. Furthermore, results on empirical human fMRI data suggest that such an approach can capture useful information about connectivity among components in the default mode network. There is a need for better characterization of underlying brain dynamics in the light of recent advances in fast fMRI acquisition techniques. We conclude that nonlinear methods that aim at accurately modeling the brains functionally interacting regions, such as MCA-LM, can provide valuable insights towards a better understanding of brain activity in both healthy and disease states.

Supplementary Material

Refer to Web version on PubMed Central for supplementary material.

Acknowledgments

This work was funded by the National Institutes of Health (NIH) Award R01-DA-034977. The content is solely the responsibility of the authors and does not necessarily represent the official views of the National Institute of Health. This work was conducted as a Practice Quality Improvement (PQI) project related to American Board of Radiology (ABR) Maintenance of Certificate (MOC) for Prof. Dr. Axel Wismüller. The authors would like to thank Dr.

Stephen Smith and Dr. Mark Woolrich for providing us the NetSim simulation software [25]. We would also like to thank the anonymous reviewers whose insightful comments helped us improve our paper. The authors would like to thank Prof. Dr. Herbert Witte of Bernstein Group for Computational Neuroscience, Jena, Institute of Medical Statistics, Computer Science and Documentation, Jena University Hospital, Friedrich Schiller University, Jena, Germany, Dr. Oliver Lange and Prof. Dr. Maximilian F. Reiser of the Institute of Clinical Radiology, Ludwig Maximilian University, Munich, Germany for their support.

References

1Biswal B, Zerrin Yetkin F, Haughton VM, Hyde JS. Functional connectivity in the motor cortex of resting human brain using echo-planar MRI. Magnetic resonance in medicine. 1995; 34(4):537–541. DOI: 10.1002/mrm.1910340409 [PubMed: 8524021]

2Damoiseaux J, Rombouts S, Barkhof F, Scheltens P, Stam C, Smith SM, Beckmann C. Consistent resting-state networks across healthy subjects. Proceedings of the national academy of sciences. 2006; 103(37):13848–13853.

3De Luca M, Beckmann C, De Stefano N, Matthews P, Smith SM. fmri resting state networks define distinct modes of long-distance interactions in the human brain. Neuroimage. 2006; 29(4):1359–1367. [PubMed: 16260155]

4Cordes D, Haughton VM, Arfanakis K, Wendt GJ, Turski PA, Moritz CH, Quigley MA, Meyerand ME. Mapping functionally related regions of brain with functional connectivity mr imaging. American Journal of Neuroradiology. 2000; 21(9):1636–1644. [PubMed: 11039342]

5Beckmann CF, DeLuca M, Devlin JT, Smith SM. Investigations into resting-state connectivity using independent component analysis. Philosophical transactions of the Royal Society of London, Series B, Biological sciences. 2005; 360(1457):1001–13. URL http://www.pubmedcentral.nih.gov/articlerender.fcgi?artid=1854918{&}tool=pmcentrez{&}rendertype=abstract. DOI: 10.1098/rstb.2005.1634 [PubMed: 16087444]

6Van Den Heuvel MP, Pol HEH. Exploring the brain network: a review on resting-state fmri functional connectivity. European neuropsychopharmacology. 2010; 20(8):519–534. [PubMed: 20471808]

7Smith SM. The future of fmri connectivity. Neuroimage. 2012; 62(2):1257–1266. [PubMed: 22248579]

8Buxton RB, Wong EC, Frank LR. Dynamics of blood flow and oxygenation changes during brain activation: The balloon model. Magnetic Resonance in Medicine. 1998; 39(6):855–864. DOI: 10.1002/mrm.1910390602 [PubMed: 9621908]

9Friston KJ, Harrison L, Penny W. Dynamic causal modelling. NeuroImage. 2003; 19(4):1273–1302. DOI: 10.1016/S1053-8119(03)00202-7 [PubMed: 12948688]

10Stam CJ. Nonlinear brain dynamics Nova Publishers; 2006

11Anzellotti S, Kliemann D, Jacoby N, Saxe R. Directed network discovery with dynamic network modelling. Neuropsychologia. 2017; 99:1–11. [PubMed: 28215697]

12Tononi G, Edelman GM, Sporns O. Complexity and coherency: Integrating information in the brain. Trends in Cognitive Sciences. 1998; 2(12):474–484. DOI: 10.1016/S1364-6613(98)01259-5 [PubMed: 21227298]

13Sporns O, Chialvo DR, Kaiser M, Hilgetag CC. Organization, development and function of complex brain networks. Trends in Cognitive Sciences. 2004; 8(9):418–425. DOI: 10.1016/j.tics.2004.07.008 [PubMed: 15350243]

14Friston KJ. Functional and effective connectivity in neuroimaging: A synthesis. Human Brain Mapping. 1994; 2(1–2):56–78. URL http://doi.wiley.com/10.1002/hbm.460020107. DOI: 10.1002/hbm.460020107

15Roebroeck A, Formisano E, Goebel R. Mapping directed influence over the brain using Granger causality and fMRI. Neuroimage. 2005; 25:230–242. DOI: 10.1016/j.neuroimage.2004.11.017 [PubMed: 15734358]

16Wismüller A, , Abidin AZ, , DSouza AM, , Nagarajan MB. Advances in Self-Organizing Maps and Learning Vector Quantization Springer; 2016 Mutual connectivity analysis (mca) for nonlinear functional connectivity network recovery in the human brain using convergent cross-mapping and non-metric clustering; 217226

17Friston KJ, Mechelli A, Turner R, Price CJ. Nonlinear responses in fmri: the balloon model, volterra kernels, and other hemodynamics. NeuroImage. 2000; 12(4):466–477. [PubMed: 10988040]

18Lombardi A, , Guccione P, , Mascolo L. 20th IMEKO TC-4 International Symposium on Measurements of Electrical Quantities Benevento; 2014 Analysis of fmri data using the complex systems approach; 1517

19Gautama T, Mandic DP, Van Hulle MM. Signal nonlinearity in fmri: a comparison between bold and mion. IEEE transactions on medical imaging. 2003; 22(5):636–644. [PubMed: 12846432]

20Minati L, Chiesa P, Tabarelli D, D'Incerti L, Jovicich J. Synchronization, non-linear dynamics and low-frequency fluctuations: analogy between spontaneous brain activity and networked single-transistor chaotic oscillators. Chaos: An Interdisciplinary Journal of Nonlinear Science. 2015; 25(3):033107.

21Gultepe E, He B. A linear/nonlinear characterization of resting state brain networks in fmri time series. Brain topography. 2013; 26(1):39–49. [PubMed: 22941499]

22Liao W, Marinazzo D, Pan Z, Gong Q, Chen H. Kernel granger causality mapping effective connectivity on fmri data. IEEE transactions on medical imaging. 2009; 28(11):1825–1835. [PubMed: 19709972]

23Karanikolas G, , Giannakis GB, , Slavakis K, , Leahy R. Multi-kernel based nonlinear models for connectivity identification of brain networks. Acoustics, Speech and Signal Processing (ICASSP); 2016 IEEE International Conference on, IEEE; 2016 63156319

24Wismüller A, Wang X, DSouza AM, Nagarajan MB. A framework for exploring non-linear functional connectivity and causality in the human brain: Mutual connectivity analysis (mca) of resting-state functional mri with convergent cross-mapping and non-metric clustering. arXiv preprint arXiv. :1407.3809.

25Smith SM, Miller KL, Salimi-Khorshidi G, Webster M, Beckmann CF, Nichols TE, Ramsey JD, Woolrich MW. Network modelling methods for FMRI. NeuroImage. 2011; 54(2):875–891. URL . DOI: 10.1016/j.neuroimage.2010.08.063 DOI: 10.1016/j.neuroimage.2010.08.063 [PubMed: 20817103]

26Sugihara G, May R, Ye H, Hsieh C-h, Deyle E, Fogarty M, Munch S. Detecting causality in complex ecosystems. science. 2012; 338(6106):496–500. [PubMed: 22997134]

27Ma H, Aihara K, Chen L. Detecting causality from nonlinear dynamics with short-term time series. Scientific reports. 4

28McBride JC. Dynamic complexity and causality analysis of scalp eeg for detection of cognitive deficits.

29Takens F. Dynamical systems and turbulence, Warwick Vol. 1980. Springer; 1981 Detecting strange attractors in turbulence; 366381

30Packard NH, Crutchfield JP, Farmer JD, Shaw RS. Geometry from a time series. Physical review letters. 1980; 45(9):712.

31Ruelle D. Chaotic evolution and strange attractors Vol. 1. Cambridge University Press; 1989

32Deyle ER, Sugihara G. Generalized theorems for nonlinear state space reconstruction. PLoS One. 2011; 6(3):e18295. [PubMed: 21483839]

33Atkeson CG, Moore AW, Schaal S. Locally weighted learning. Artificial intelligence review. 1997; 11(1–5):11–73.

34Sugihara G, May RM. Nonlinear forecasting as a way of distinguishing chaos from, Nonlinear Physics for Beginners: Fractals, Chaos, Solitons, Pattern Formation. Cellular Automata and Complex Systems. 1998:118.

35Tajima S, Yanagawa T, Fujii N, Toyoizumi T. Untangling brain-wide dynamics in consciousness by cross-embedding. PLoS computational biology. 2015; 11(11):e1004537. [PubMed: 26584045]

36Ramsey JD, Hanson SJ, Glymour C. Multi-subject search correctly identifies causal connections and most causal directions in the dcm models of the smith et al. simulation study. NeuroImage. 2011; 58(3):838–848. [PubMed: 21745580]

37Mumford JA, Ramsey JD. Bayesian networks for fmri: a primer. Neuroimage. 2014; 86:573–582. [PubMed: 24140939]

38Iyer SP, Shafran I, Grayson D, Gates K, Nigg JT, Fair DA. Inferring functional connectivity in mri using bayesian network structure learning with a modified pc algorithm. Neuroimage. 2013; 75:165–175. [PubMed: 23501054]

39Seth AK, Chorley P, Barnett LC. Granger causality analysis of fmri bold signals is invariant to hemodynamic convolution but not downsampling. Neuroimage. 2013; 65:540–555. [PubMed: 23036449]

40Ramsey JD, Sanchez-Romero R, Glymour C. Non-gaussian methods and high-pass filters in the estimation of effective connections. Neuroimage. 2014; 84:986–1006. [PubMed: 24099845]

41Behzadi Y, Restom K, Liau J, Liu TT. A component based noise correction method (compcor) for bold and perfusion based fmri. Neuroimage. 2007; 37(1):90–101. [PubMed: 17560126]

42Sikka S, , Cheung B, , Khanuja R, , Ghosh S, , Yan C, , Li Q, , Vogelstein J, , Burns R, , Colcombe S, , Craddock C. , et al. 5th INCF Congress of Neuroinformatics Vol. 10. Munich; Germany: 2014Towards automated analysis of connectomes: The configurable pipeline for the analysis of connectomes (c-pac).

43Smith SM, Jenkinson M, Woolrich MW, Beckmann CF, Behrens TE, Johansen-Berg H, Bannister PR, De Luca M, Drobnjak I, Flitney DE, et al. Advances in functional and structural MR image analysis and implementation as FSL. NeuroImage. 2004; 23(Suppl 1):S208–19. DOI: 10.1016/j.neuroimage.2004.07.051 [PubMed: 15501092]

44Wismüller A, Lange O, Dersch DR, Leinsinger GL, Hahn K, Pütz B, Auer D. Cluster analysis of biomedical image time-series. International Journal of Computer Vision. 2002; 46(2):103–128. DOI: 10.1023/A:1013550313321

45Marrelec G, Krainik A, Duffau H, Pélégrini-Issac M, Lehéricy S, Doyon J, Benali H. Partial correlation for functional brain interactivity investigation in functional mri. Neuroimage. 2006; 32(1):228–237. [PubMed: 16777436]

46Patel RS, Bowman FD, Rilling JK. A bayesian approach to determining connectivity of the human brain. Human brain mapping. 2006; 27(3):267–276. [PubMed: 16092131]

47Granger CW. Investigating causal relations by econometric models and cross-spectral methods. Econometrica: Journal of the Econometric Society. 1969:424–438.

48Shannon CE. A mathematical theory of communication. ACM SIGMOBILE Mobile Computing and Communications Review. 2001; 5(1):3–55.

49Grinsted A, Moore JC, Jevrejeva S. Application of the cross wavelet transform and wavelet coherence to geophysical time series. Nonlinear processes in geophysics. 2004; 11(5/6):561–566.

50Cao L. Practical method for determining the minimum embedding dimension of a scalar time series. Physica D: Nonlinear Phenomena. 1997; 110(1–2):43–50.

51Raichle ME, MacLeod AM, Snyder AZ, Powers WJ, Gusnard DA, Shulman GL. A default mode of brain function. Proceedings of the National Academy of Sciences. 2001; 98(2):676–682.

52Leech R, Sharp DJ. The role of the posterior cingulate cortex in cognition and disease. Brain. 2014; 137(1):12–32. [PubMed: 23869106]

53Fransson P, Marrelec G. The precuneus/posterior cingulate cortex plays a pivotal role in the default mode network: Evidence from a partial correlation network analysis. Neuroimage. 2008; 42(3):1178–1184. [PubMed: 18598773]

54Greicius MD, Krasnow B, Reiss AL, Menon V. Functional connectivity in the resting brain: a network analysis of the default mode hypothesis. Proceedings of the National Academy of Sciences. 2003; 100(1):253–258.

55Buckner RL, Sepulcre J, Talukdar T, Krienen FM, Liu H, Hedden T, Andrews-Hanna JR, Sperling RA, Johnson KA. Cortical hubs revealed by intrinsic functional connectivity: mapping, assessment of stability, and relation to alzheimer's disease. Journal of Neuroscience. 2009; 29(6):1860–1873. [PubMed: 19211893]

56Bluhm RL, Miller J, Lanius RA, Osuch EA, Boksman K, Neufeld R, Théberge J, Schaefer B, Williamson P. Spontaneous low-frequency fluctuations in the bold signal in schizophrenic patients: anomalies in the default network. Schizophrenia bulletin. 2007; 33(4):1004–1012. [PubMed: 17556752]

57Kennedy DP, Courchesne E. The intrinsic functional organization of the brain is altered in autism. Neuroimage. 2008; 39(4):1877–1885. [PubMed: 18083565]

58Kim J, Whyte J, Patel S, Avants B, Europa E, Wang J, Slattery J, Gee JC, Coslett HB, Detre JA. Resting cerebral blood ow alterations in chronic traumatic brain injury: an arterial spin labeling perfusion fmri study. Journal of neurotrauma. 2010; 27(8):1399–1411. [PubMed: 20528163]

59Mayer AR, Mannell MV, Ling J, Gasparovic C, Yeo RA. Functional connectivity in mild traumatic brain injury. Human brain mapping. 2011; 32(11):1825–1835. [PubMed: 21259381]

60Sharp DJ, Beckmann CF, Greenwood R, Kinnunen KM, Bonnelle V, De Boissezon X, Powell JH, Counsell SJ, Patel MC, Leech R. Default mode network functional and structural connectivity after traumatic brain injury. Brain. 2011; 134(8):2233–2247. [PubMed: 21841202]

61Bonnelle V, Leech R, Kinnunen KM, Ham TE, Beckmann CF, De Boissezon X, Greenwood RJ, Sharp DJ. Default mode network connectivity predicts sustained attention deficits after traumatic brain injury. Journal of Neuroscience. 2011; 31(38):13442–13451. [PubMed: 21940437]

62Bonnelle V, Ham TE, Leech R, Kinnunen KM, Mehta MA, Greenwood RJ, Sharp DJ. Salience network integrity predicts default mode network function after traumatic brain injury. Proceedings of the National Academy of Sciences. 2012; 109(12):4690–4695.

63Joshi AA, , Salloum R, , Bhushan C, , Leahy RM. International Conference on Information Processing in Medical Imaging Springer; 2015 Measuring asymmetric interactions in resting state brain networks; 399410

64Greicius MD, Srivastava G, Reiss AL, Menon V. Default-mode network activity distinguishes alzheimer's disease from healthy aging: evidence from functional mri. Proceedings of the National Academy of Sciences of the United States of America. 2004; 101(13):4637–4642. [PubMed: 15070770]

65Calhoun V, , Adali T. Group ica of fmri toolbox (gift) Online at http://icatb. sourceforge.net

66Tzourio-Mazoyer N, Landeau B, Papathanassiou D, Crivello F, Etard O, Delcroix N, Mazoyer B, Joliot M. Automated anatomical labeling of activations in spm using a macroscopic anatomical parcellation of the mni mri single-subject brain. Neuroimage. 2002; 15(1):273–289. [PubMed: 11771995]

67Greicius MD, Flores BH, Menon V, Glover GH, Solvason HB, Kenna H, Reiss AL, Schatzberg AF. Resting-state functional connectivity in major depression: abnormally increased contributions from subgenual cingulate cortex and thalamus. Biological psychiatry. 2007; 62(5):429–437. [PubMed: 17210143]

68Schreiber T, Schmitz A. Improved surrogate data for nonlinearity tests. Physical Review Letters. 1996; 77(4):635. [PubMed: 10062864]

69https://www.mathworks.com/matlabcentral/fileexchange/1597-chaotic-systems-toolbox.

70Smith SM, Beckmann CF, Andersson J, Auerbach EJ, Bijsterbosch J, Douaud G, Duff E, Feinberg DA, Griffanti L, Harms MP, et al. Resting-state fmri in the human connectome project. Neuroimage. 2013; 80:144–168. [PubMed: 23702415]

71Feinberg DA, Yacoub E. The rapid development of high speed, resolution and precision in fmri. Neuroimage. 2012; 62(2):720–725. [PubMed: 22281677]

72Finsterbusch J. Simultaneous functional mri acquisition of distributed brain regions with high temporal resolution using a 2d-selective radiofrequency excitation. Magnetic resonance in medicine. 2015; 73(2):683–691. [PubMed: 24574142]

73Mill RD, Bagic A, Bostan A, Schneider W, Cole MW. Empirical validation of directed functional connectivity. NeuroImage. 2017; 146:275–287. [PubMed: 27856312]

74Hagmann P, Cammoun L, Gigandet X, Meuli R, Honey CJ, Wedeen VJ, Sporns O. Mapping the structural core of human cerebral cortex. PLoS biology. 2008; 6(7):e159. [PubMed: 18597554]

75Buckner RL, Andrews-Hanna JR, Schacter DL. The brain's default network. Annals of the New York Academy of Sciences. 2008; 1124(1):1–38. [PubMed: 18400922]

76Runyan CA, Piasini E, Panzeri S, Harvey CD. Distinct timescales of population coding across cortex. Nature. 2017; 548(7665):92–96. [PubMed: 28723889]

77Baldassano C, Chen J, Zadbood A, Pillow JW, Hasson U, Norman KA. Discovering event structure in continuous narrative perception and memory. bioRxiv. 2016:081018.

78Chaudhuri R, Knoblauch K, Gariel M-A, Kennedy H, Wang X-J. A large-scale circuit mechanism for hierarchical dynamical processing in the primate cortex. Neuron. 2015; 88(2):419–431. [PubMed: 26439530]

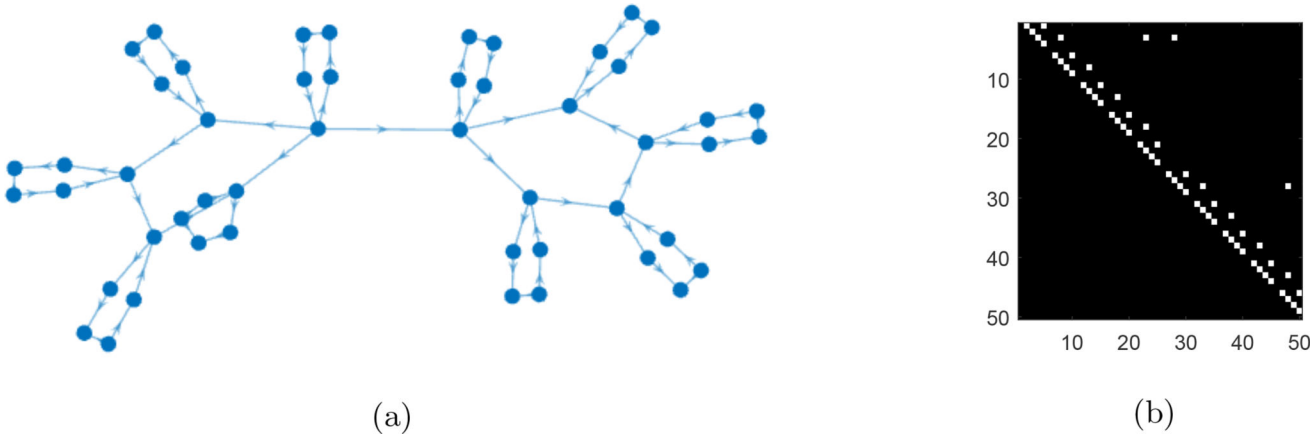

Figure 1.

Network structure adopted from [25]. Figure (a) represents the connections as a network graph and Figure (b) represents the connections as a network matrix. We construct 50 different networks for each repetition time (TR) having the same structure as is seen in this figure but with different connection strengths. Figure 2 shows all the network topologies adopted.

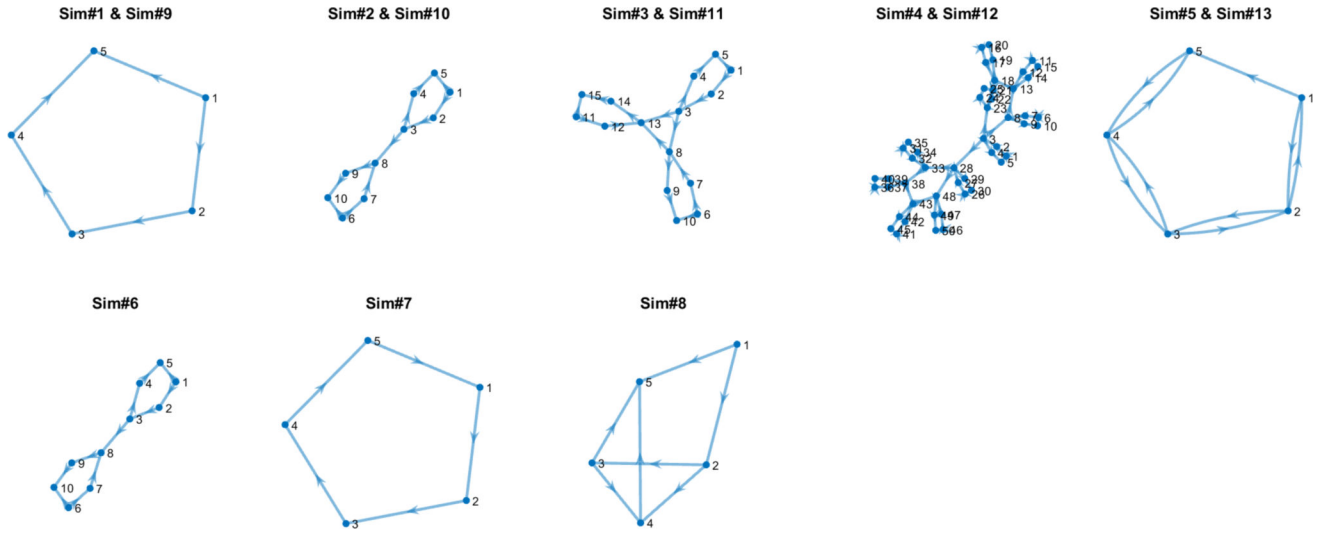

Figure 2.

Network topologies of all the simulations adopted in this paper. Sim#1 and sim#9, sim#2 and sim#10, sim#3 and sim#11, sim#4 and sim#12, and sim#5 and sim#13 have the same network topologies but differ in neural interaction strength as indicated in Table 1.

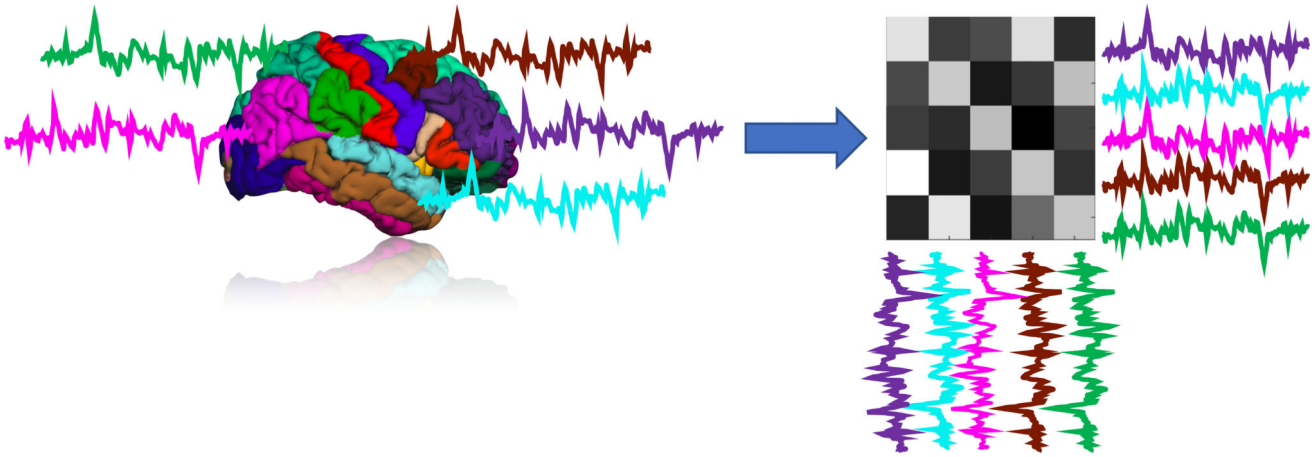

Figure 3.
Illustration demostrating connectivity analysis of fMRI time-series. Connectivity analysis estimates a measure of interactions between fMRI time-series, represented as a matrix of interactions.

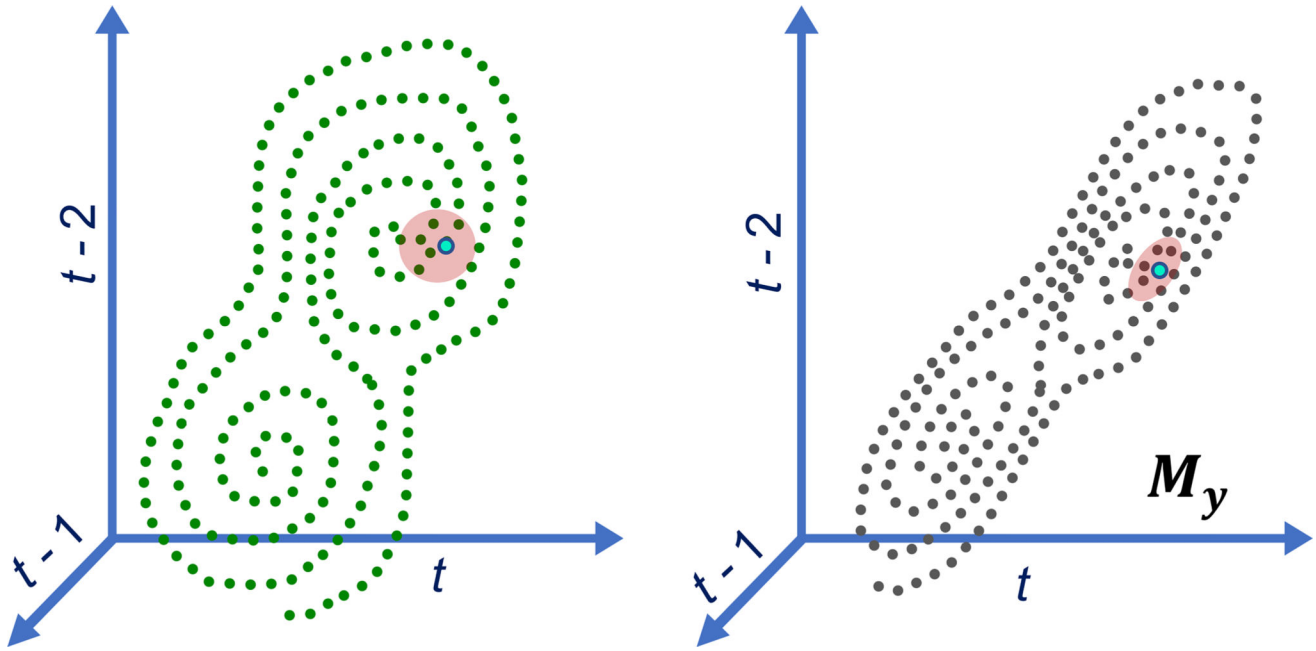

Figure 4.

Diagramatic representation of cross-mapping from $\boldsymbol{M}_{\mathbf{x}}$ to $\boldsymbol{M}_{\mathbf{y}}$. In this illustration, the nearest neighbors (represented in the red circle) of $\mathbf{x}_t$ (blue dot) map to the nearest neighbors of $\mathbf{y}_t$. This situation occurs when **y** influences **x**. However, if this is not the case, nearest neighbors of $\mathbf{x}_t$ would not map to nearest neighbors of $\mathbf{y}_t$.

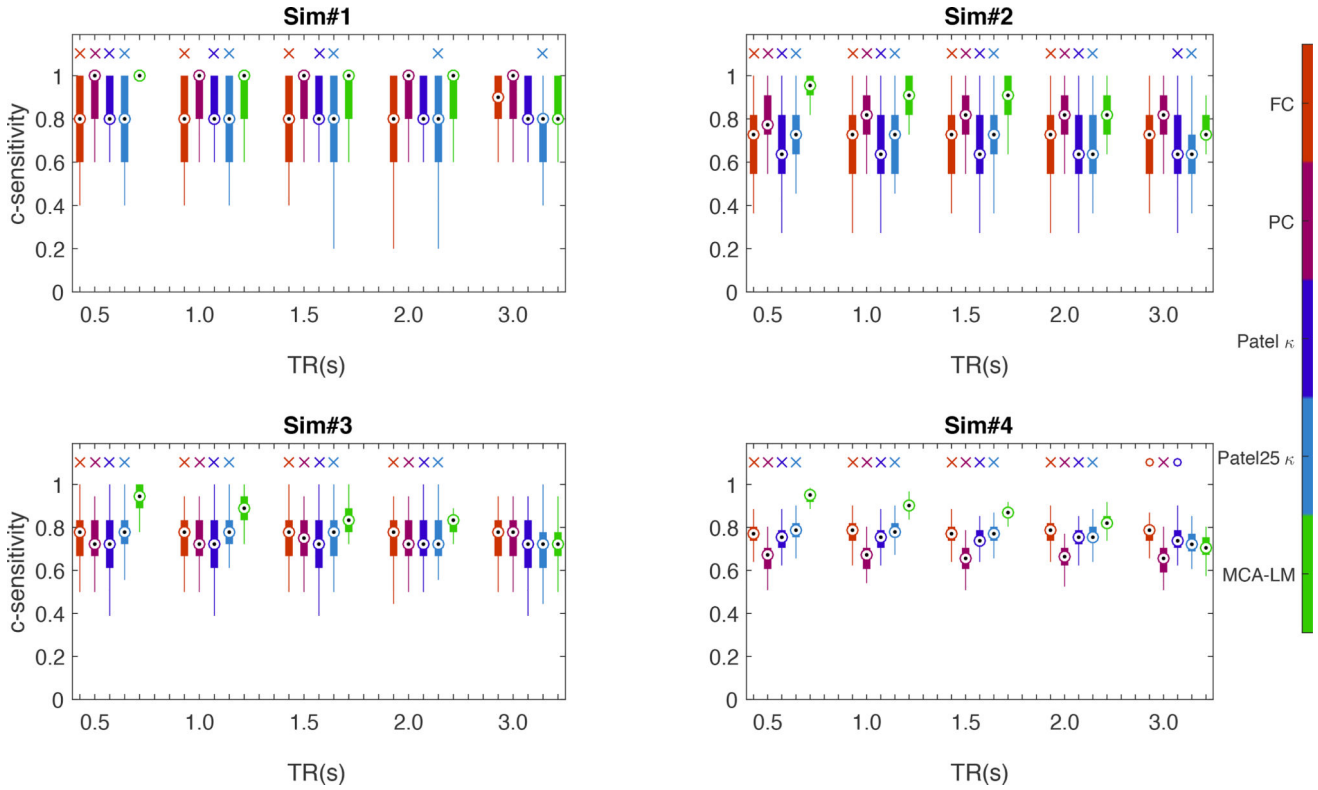

Figure 5.

C-sensitivity results on simulations 1 to 4 for different TR and different approaches visualized as boxplots. The bottom end of the box represents the first quartile and the top of the box represents the third quartile. Sim#1 through sim#4 have increasing number of nodes. Details are provided in Table 1. The circle with a dot in the box represents the distribution median. The 'x' sign of a particular color indicates if MCA-LM is significantly ($p < 0.01$) better than the plot of the corresponding color and 'o' indicates if it is significantly worse. At low TR, MCA-LM performs better than correlation-based methods (CM). Performance drops for all approaches as the number of nodes increases.

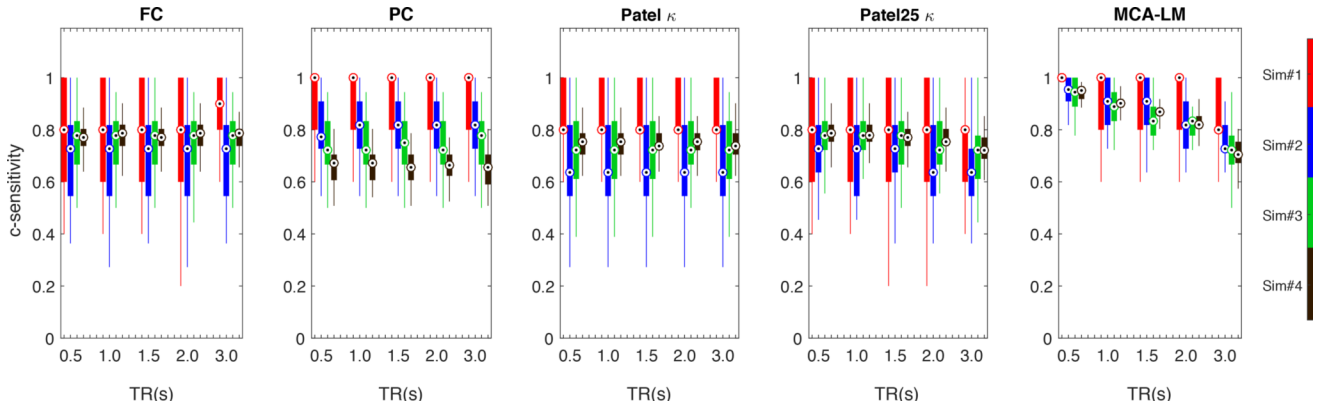

Figure 6.

This figure represents the same information present in Figure 5, however, here we compare performance of the methods with increasing number of nodes. Sim#1 through to sim#4 have 5, 10, 15, 50 nodes respectively. C-sensitivity results on the simulations are visualized as boxplots for different TR. The bottom end of the box represents the first quartile and the top end represents the third quartile. The circle In the box represents the distribution median. At low TR, performance of MCA-LM does not reduce much with increasing number of nodes.

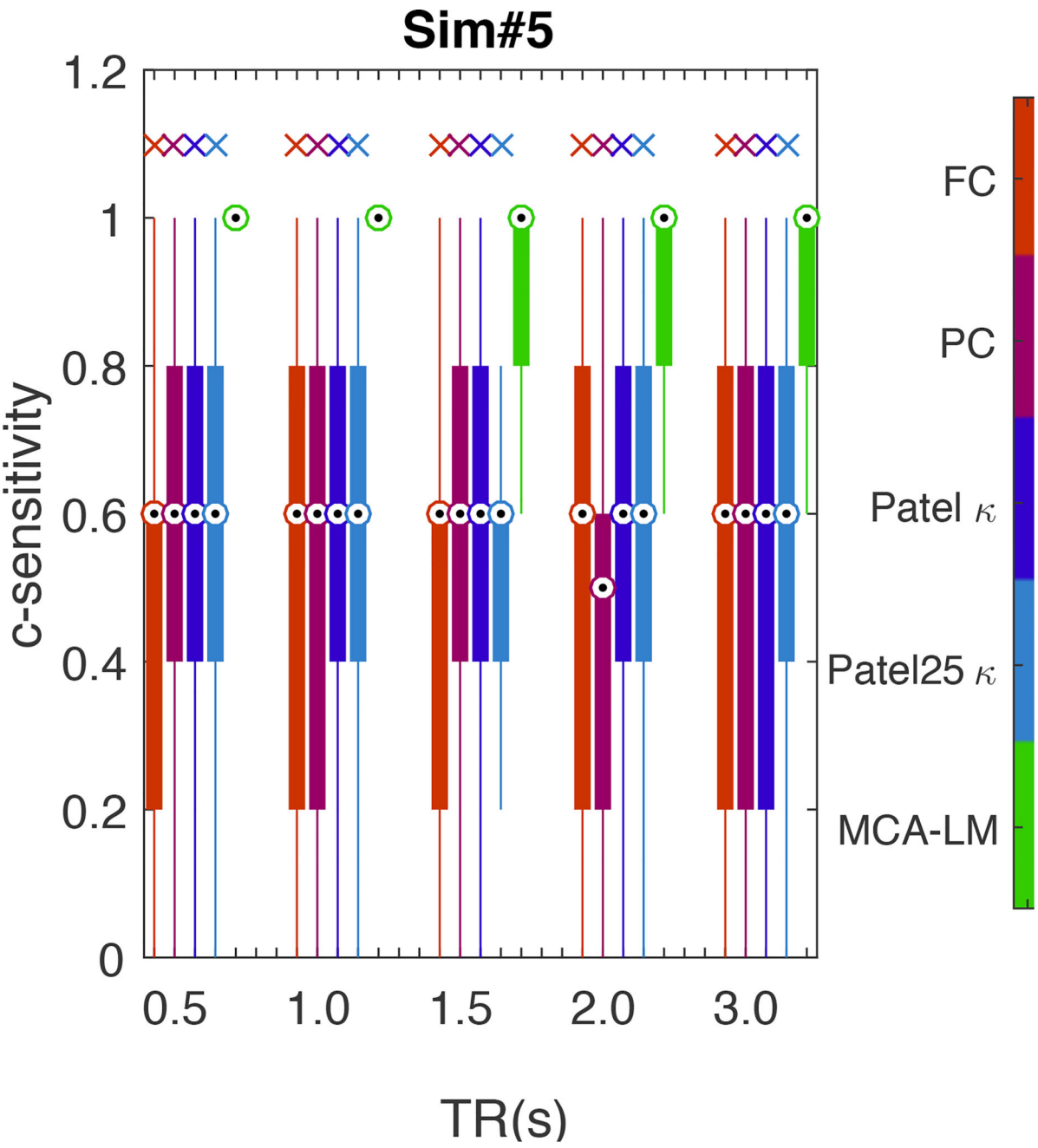

Figure 7.

C-sensitivity results on simulation 5 for different TR and different approaches visualized as boxplots. The bottom end of the box represents the first quartile and the top of the box represents the third quartile. The circle with a dot in the box represents the distribution median. This simulation accounts for bidirectional, inhibitory and excitatory connections. The 'x' sign of a particular color indicates if MCA-LM is significantly ($p < 0.01$) better than the plot of the corresponding color. MCA-LM clearly performs better than the other approaches for all TRs.

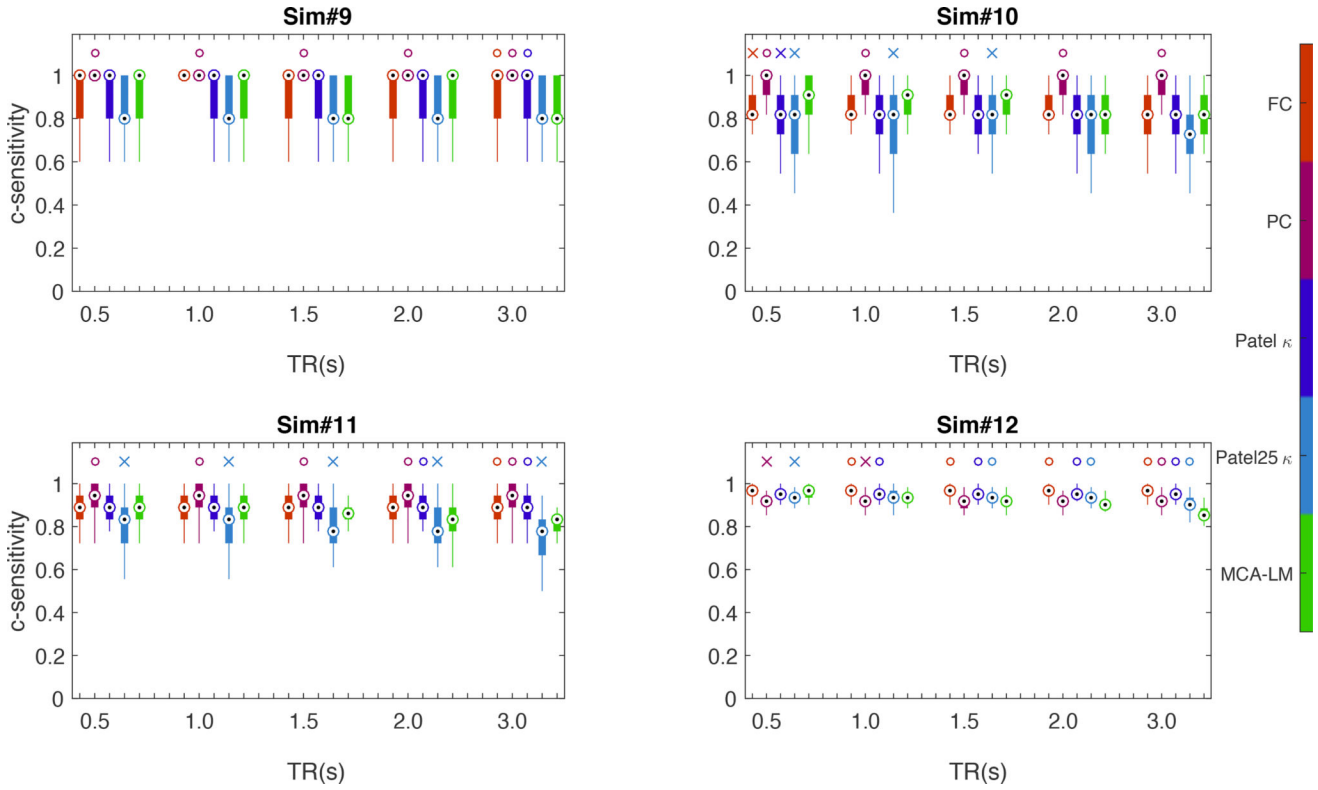

Figure 8.

C-sensitivity results on simulations 9 to 12 for different TR with 0.1% noise and different approaches visualized as boxplots. The bottom end of the box represents the first quartile and the top of the box represents the third quartile. The circle with a dot in the box represents the distribution median. The 'x' sign of a particular color indicates if MCA-LM is significantly ($p < 0.01$) better than the plot of the corresponding color and 'o' indicates if it is significantly worse. MCA-LM and the other approaches perform well. These simulations differ from sim#1 to sim#4 (at noise = 0.1%) in only connection strength.

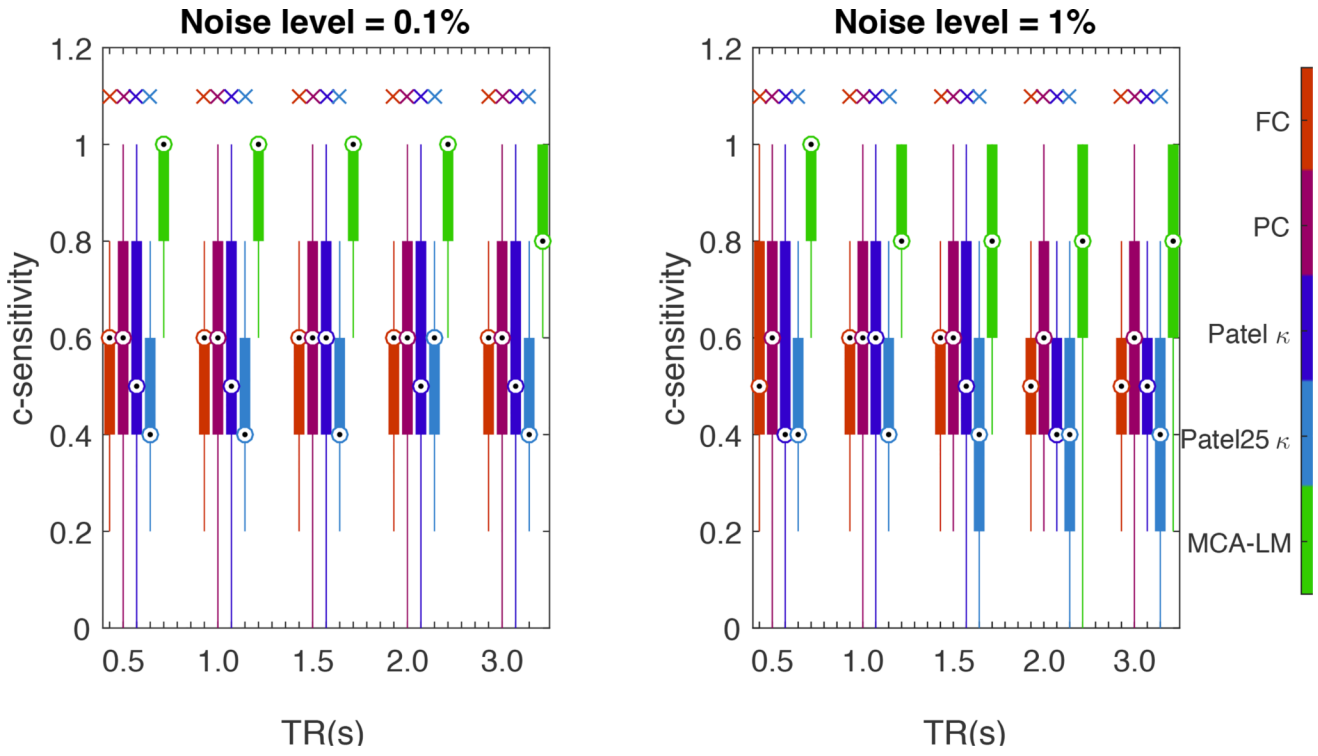

Figure 9.

C-sensitivity results on sim#13 for different TR and different approaches visualized as boxplots. The bottom end of the box represents the first quartile and the top of the box represents the third quartile. The circle with a dot in the box represents the distribution median. The 'x' sign of a particular color indicates if LM is significantly ($p < 0.01$) better than the plot of the corresponding color. Sim#13 models excitatory and inhibitory connections. For such a simulation, MCA-LM clearly performs better than the other approaches for high and low noise.

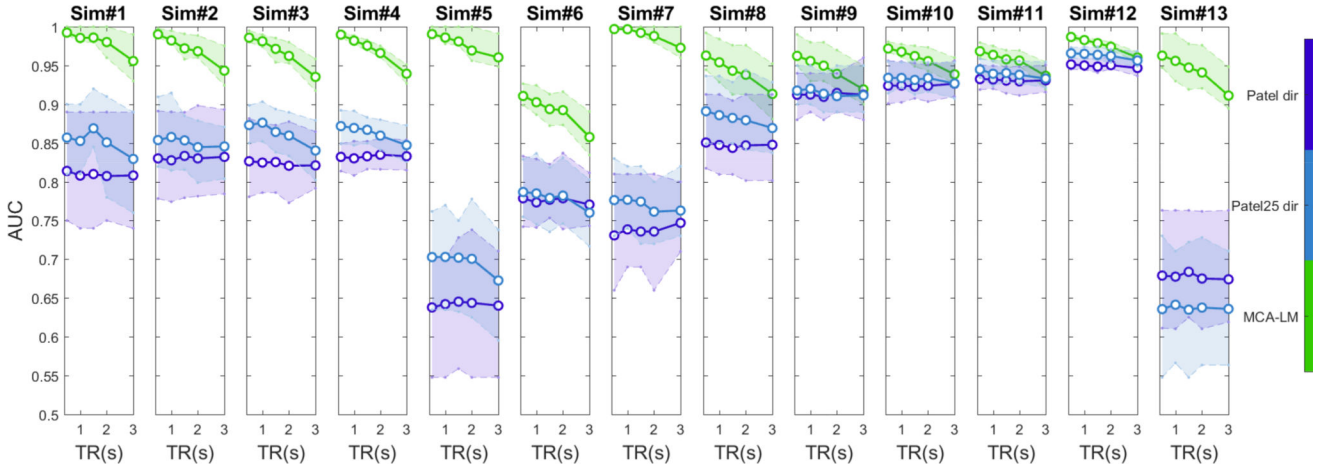

Figure 10.

Plots showing the AUC obtained when comparing the presence or absence of network connections recovered by MCA-LM and Patel's measures with the known network ground truth for the various simulations. The (1) Green plot corresponds MCA-LM, (2) Dark blue to Patel directed and (3) Light blue to Patel25 directed. The bold line represents the median AUC while the shaded portions correspond to the interquartile range. Observe that for MCA-LM, in nearly all cases the AUC is above 0.90. Also, the AUC drops steadily with increasing TR.

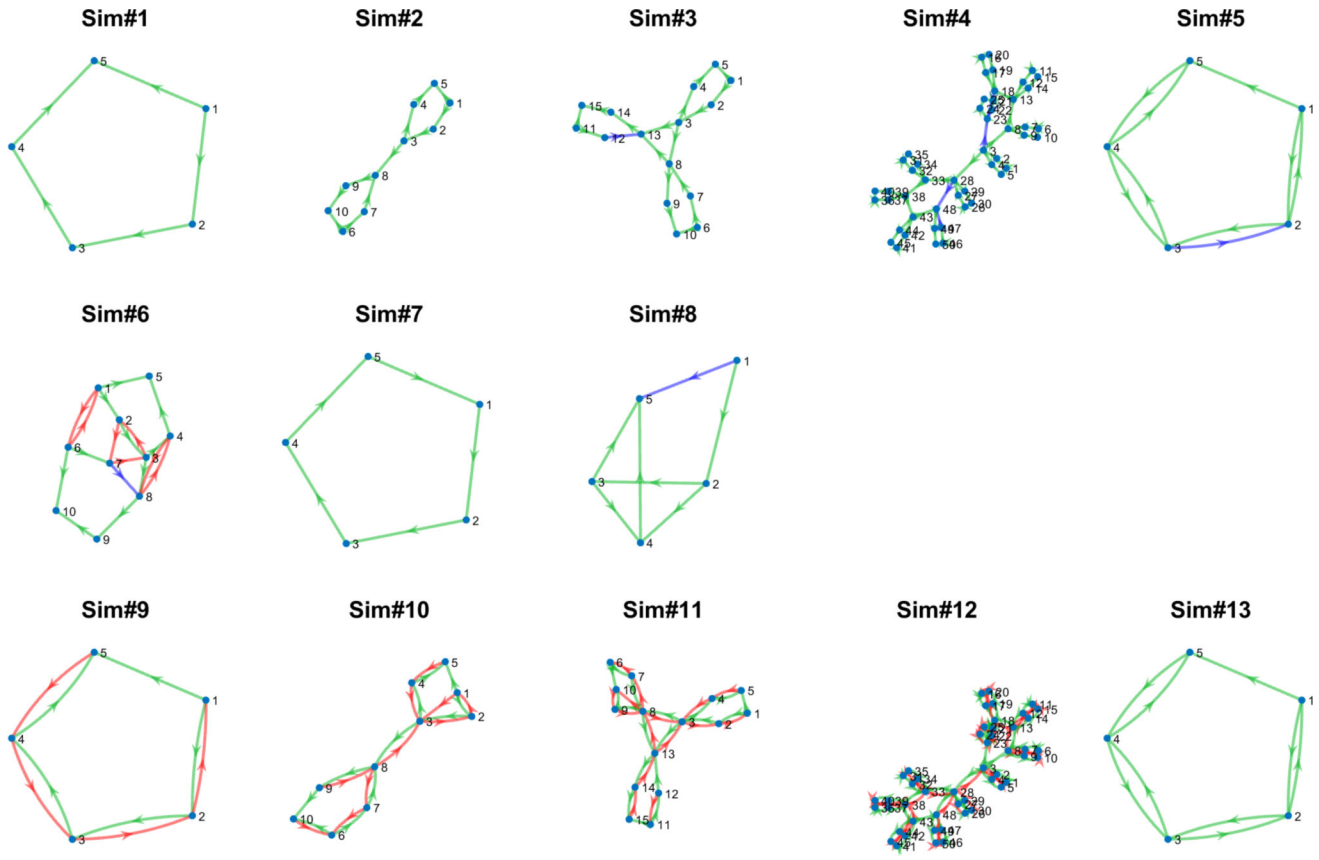

Figure 11.

Graphical representation of network structures recovered with MCA-LM for simulations 1 to 13 at TR = 2 s. Graphs were obtained for each simulation after thresholding the average affinity matrix obtained for all trials at $p < 0.01$. Green, red and blue arrows indicates right connection, false connection and missed connection respectively.

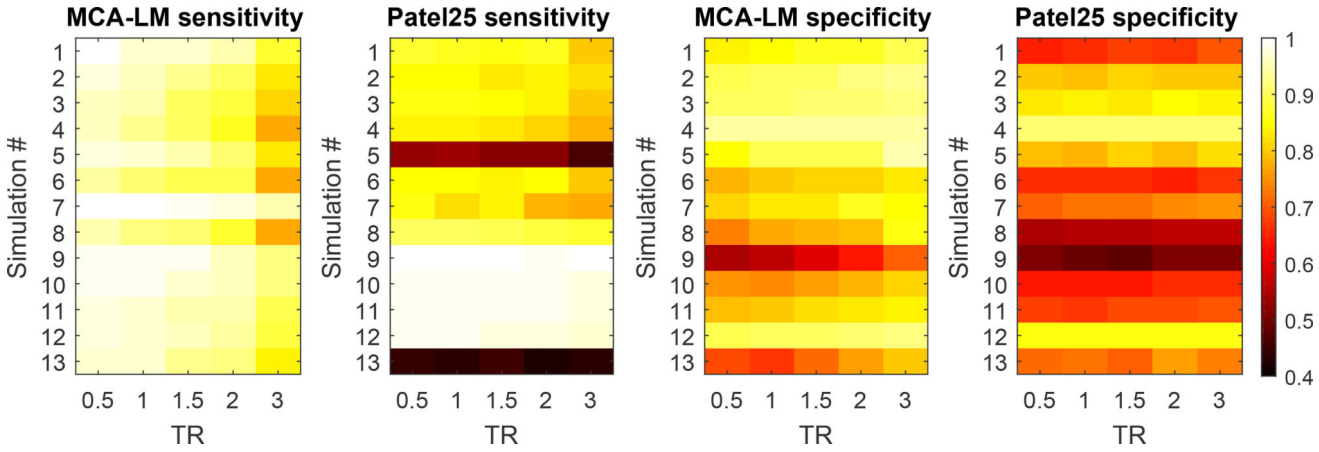

Figure 12.

Heatmap comparing average sensitivity and specificity measures obtained with MCA-LM and Patel25 directed connectivity matrix. We clearly see that Patel's measures do not work well for simulation 5 and 13 which correspond to simulations with backward connections. Additionally, its performance does not change with TR.

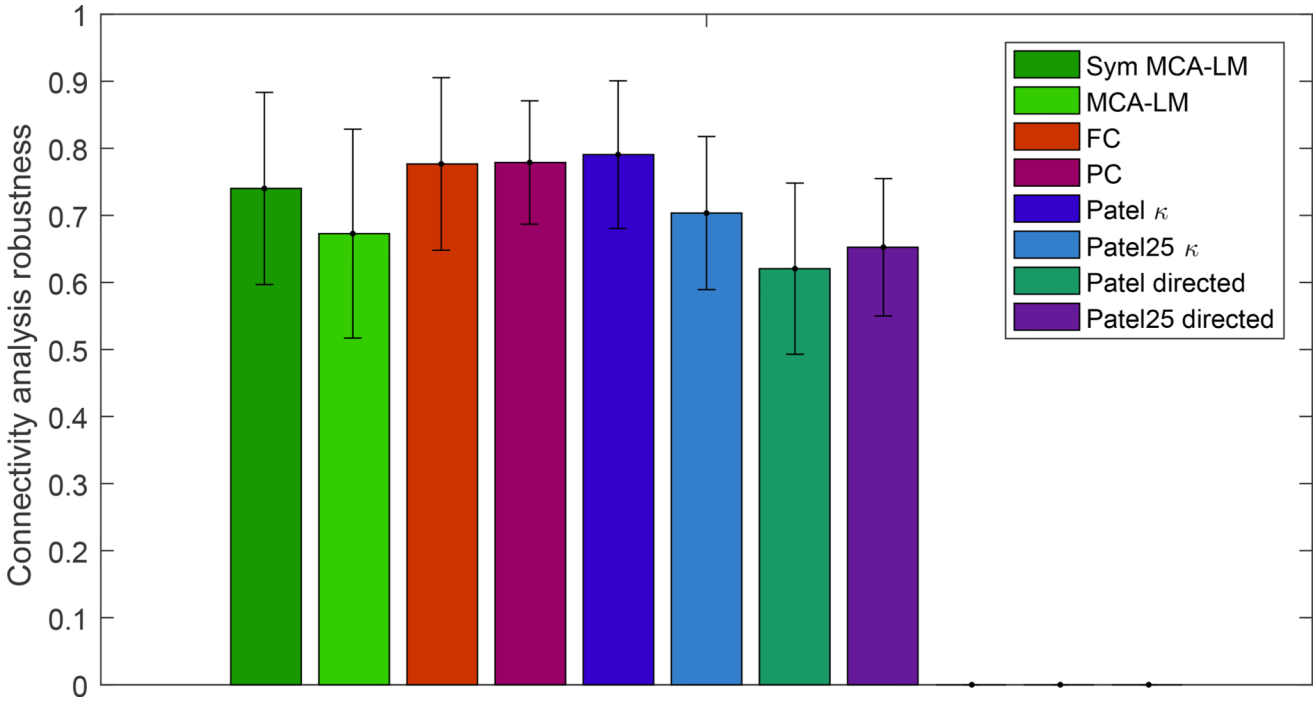

Figure 13.

Comparing robustness of connectivity analysis approaches in estimating connectivity profiles for two fMRI scans of every subject measured with Pearson's correlation coefficient. The bar corresponds to the mean of correlation for the 14 subjects, and the error bar is one standard deviation above and below the mean.

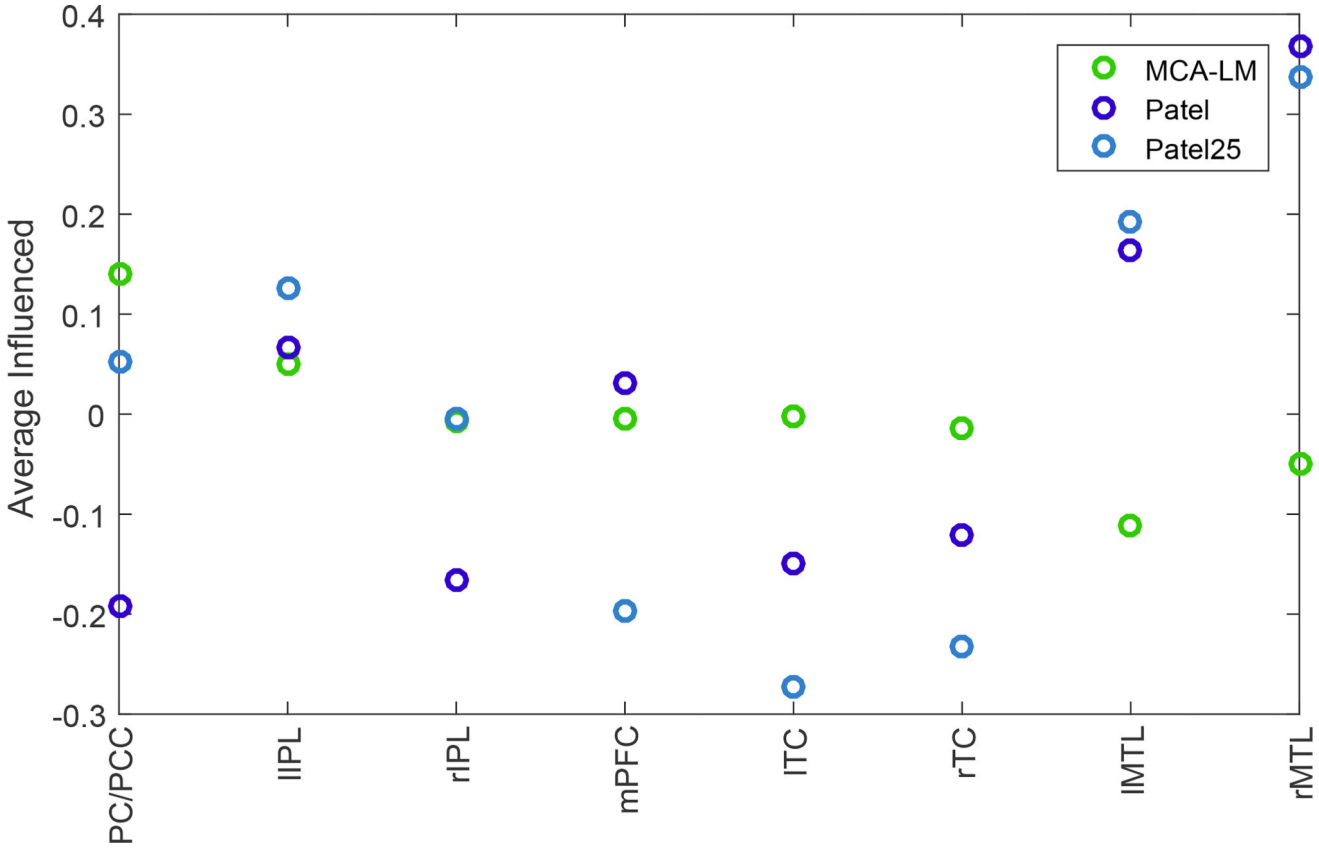

Figure 14.

Plot shows the average amount each of the eight nodes in the DMN are influenced by other nodes. Positive value indicates a node being influenced strongly while negative value represents an influencer node.

Table 1

FMRI simulation parameters summary

Sim. (#)	No. of nodes	Sess. length (min)	TR (min)	Noise (%)	Connection strength	Other factors
1	5	10	{0.5, 1, 1.5, 2, 3}	0.1	Weak	
2	10	10	{0.5, 1, 1.5, 2, 3}	0.1	Weak	
3	15	10	{0.5, 1, 1.5, 2, 3}	0.1	Weak	
4	50	10	{0.5, 1, 1.5, 2, 3}	0.1	Weak	
5	5	10	{0.5, 1, 1.5, 2, 3}	0.1	Weak	Backward conn.
6	10	10	{0.5, 1, 1.5, 2, 3}	0.1	Weak	Bad ROIs
7	5	10	{0.5, 1, 1.5, 2, 3}	0.1	Weak	Cyclic conn.
8	5	10	{0.5, 1, 1.5, 2, 3}	0.1	Weak	Dense conn.
9	5	10	{0.5, 1, 1.5, 2, 3}	{0.1, 1.0}	Moderate	
10	10	10	{0.5, 1, 1.5, 2, 3}	{0.1, 1.0}	Moderate	
11	15	10	{0.5, 1, 1.5, 2, 3}	{0.1, 1.0}	Moderate	
12	50	10	{0.5, 1, 1.5, 2, 3}	{0.1, 1.0}	Moderate	
13	10	10	{0.5, 1, 1.5, 2, 3}	{0.1, 1.0}	Moderate	Backward conn.